North African dust export and deposition: A satellite and model perspective

D. A. Ridley,[1] C. L. Heald,[1] and B. Ford[1]

Received 29 August 2011; revised 27 October 2011; accepted 15 November 2011; published 20 January 2012.

[1] We use a suite of satellite observations (Moderate Resolution Imaging Spectroradiometer (MODIS), Multiangle Imaging Spectroradiometer (MISR), Cloud-Aerosol Lidar With Orthogonal Polarization (CALIOP)) to investigate the processes of long-range transport of dust represented in the global GEOS-Chem model in 2006–2008. A multiyear mean of African dust transport is developed and used to test the representation of the variability in the model. We find that both MODIS and MISR correlate well with the majority of Aerosol Robotic Network observations in the region ($r > 0.8$). However, MODIS aerosol optical depth (AOD) appears to be biased low (>0.05) relative to MISR in Saharan regions during summer. We find that GEOS-Chem captures much of the variability in AOD when compared with MISR and MODIS ($r > 0.6$) and represents the vertical structure in aerosol extinction over outflow regions well when compared to CALIOP. Including a realistic representation of the submicron-size distribution of dust reduces simulated AOD by ~25% over North Africa and improves agreement with observations. The lifetime of the simulated dust is typically a few days (25%–50%) shorter than inferred from MODIS observations, suggesting overvigorous wet removal, confirmed by comparison with rain rate observations from the Tropical Rainfall Measuring Mission satellite. The simulation captures the seasonality of deposition in Florida and the observed magnitude and variability of dust concentrations at Barbados from 2006 to 2008 ($r = 0.74$), indicating a good simulation of the impacts of North African dust on air quality in North America. We estimate that 218 ± 48 Tg of dust is annually deposited into the Atlantic and calculate a lower estimate for the dust deposited in the Caribbean and Amazon to be 26 ± 5 Tg yr^{-1} and 17 ± 5 Tg yr^{-1}, respectively. This suggests that the dust deposition in the Amazon derived from satellites may be an upper limit.

Citation: Ridley, D. A., C. L. Heald, and B. Ford (2012), North African dust export and deposition: A satellite and model perspective, *J. Geophys. Res.*, *117*, D02202, doi:10.1029/2011JD016794.

1. Introduction

[2] Mineral dust is arguably the most important aerosol in terms of the impact upon the radiation budget in equatorial regions, with Africa contributing approximately half of the world's mineral dust aerosol [*Ginoux et al.*, 2004]. These aerosols have important effects not only on local air quality, visibility, and the radiative budget [*Li et al.*, 2004; *Sokolik and Toon*, 1996; *Tegen and Lacis*, 1996], but also on the atmosphere and ecosystems around the world. Significant quantities of dust are deposited into the Atlantic Ocean where they act as a nutrient source for phytoplankton [*Jickells et al.*, 2005; *Mahowald et al.*, 2005b]; however, dust often reaches as far as South America, the Caribbean, and the southern United States, where it degrades air quality [*Gyan et al.*, 2005; *Prospero*, 1999; *Prospero et al.*, 2001] and, in the case of the Amazon, provides a much needed nutrient source of minerals for the rain forest [*Swap et al.*, 1992]. In the Amazon the thick vegetation, frequent flooding, and lack of recent volcanic activity result in nutrient deficient soils. It has been suggested that important nutrients present in mineral dust, such as phosphorus, potassium, and iron, are delivered to the Amazon from dust storms in the Sahara and Sahel region [*Bristow et al.*, 2010; *Koren et al.*, 2006].

[3] Dust emission from these regions varies on daily to annual time scales, being influenced primarily by the changing surface vegetation cover, the wind speed and the soil moisture. Dust particles are lofted when wind exceeds a critical threshold, causing the smallest particles to be suspended in the air and larger particles to creep (roll) and saltate (bounce) which further frees more small particles [*Gillette and Passi*, 1988; *Ravi et al.*, 2011]. Conditions leading to dust uplift include synoptic-scale systems, downward mixing from nocturnal low-level jets, boundary layer convection, "haboobs" (cold pools formed from evaporation during convective storms) and dust devils

[1]Department of Atmospheric Science, Colorado State University, Fort Collins, Colorado, USA.

0148-0227/12/2011JD016794

[*Knippertz*, 2008; *Marsham et al.*, 2008, 2011]. There have been several schemes developed to parameterize the processes determining dust availability, and convert surface mass to vertical mass flux for global models [*Ginoux et al.*, 2001; *Nickovic et al.*, 2000; *Zender et al.*, 2003a, 2003b]. Once dust aerosol is lofted the long-range transport from Africa is influenced by the direction of the trade winds across the Atlantic, with African dust reaching North America in summer and South America in winter/spring as the Intertropical Convergence Zone (ITCZ) shifts southward. The deposition of African dust far from source has been monitored at sites across the Americas revealing that African dust can contribute significantly to air quality degradation far from source [*Prospero et al.*, 1981, 2005; *Reid et al.*, 2003]. Individual dust plumes have previously been tracked and studied in several campaigns over Africa, such as DABEX [*Haywood et al.*, 2008], SAFARI [*Haywood et al.*, 2003b], and SHADE [*Tanré et al.*, 2003] using aircraft and ground station measurements, such as the Aerosol Robotic Network (AERONET) Sun photometers. Several modeling studies have taken a case-by-case approach, simulating long-range transport of dust plumes across the Atlantic and using satellite observations to test aerosol models' ability to capture these features [*Generoso et al.*, 2008; *Kalashnikova and Kahn*, 2008; *Laurent et al.*, 2010; *Martet et al.*, 2009]. However, a limited number of studies have investigated the accuracy of model simulations over seasonal time scales or longer [*Ginoux et al.*, 2004; *Yu et al.*, 2010].

[4] Although the quantity of dust reaching the Amazon has previously been evaluated from aircraft and satellite observations [*Kaufman et al.*, 2005; *Koren et al.*, 2006; *Swap et al.*, 1992] there has not previously been an assessment from a modeling study. In this study we bring together a suite of observations to characterize the lifetime and behavior of African dust from 2006–2008 on daily to annual time scales. These data are then used to test a new representation of the submicron dust aerosol in the GEOS-Chem model, the model's ability to simulate the long-range transport of aerosol to the Americas, and aid a better understanding of the important underlying processes.

2. Observational Dust Climatology

2.1. Description of Observations

[5] To build a picture of how African dust export varies over different time scales we have employed several different observational platforms. We use aerosol optical depth (AOD) derived from Sun photometers in Africa that form part of the AERONET global aerosol monitoring network [*Holben et al.*, 1998]. AERONET reports daytime AOD and related aerosol properties (size distribution, single scattering albedo, etc.) at four or more wavelengths in the visible and near IR. These direct measurements have been used as the primary validation tool for satellite AOD and models [*Chu et al.*, 2002; *Kahn et al.*, 2005; *Kinne et al.*, 2003; *Remer et al.*, 2002]. The AERONET Version 2 hourly level 2 data are used to derive daily AOD for 2006–2008 and also 2 h averages at the time of satellite overpass. The AOD retrievals at 440 nm and 670 nm are linearly interpolated to 550 nm for comparison with MISR, MODIS and GEOS-Chem (interpolation yields results within 1.5% of the AOD calculated using the angstrom exponent for 95% of the data and is therefore an acceptable approximation for this study). Locations of the eight sites examined here are shown in Figure 1.

[6] Moderate-Resolution Imaging Spectroradiometer (MODIS) instruments were launched aboard both the Terra and Aqua NASA satellites and provide continuous measurements from 2000 and 2002, respectively. The device provides multiband measurements over ocean and land surface allowing retrieval of aerosol optical properties [*Remer et al.*, 2005a]. The wide swath (2330 km) and Sun-synchronous orbit allows for complete coverage of the Earth every 1–2 days, with daytime equator crossings at 1030 and 1330 for MODIS Terra and Aqua, respectively. The retrieved AOD (τ) is estimated to be accurate to $0.03 \pm 0.05\tau$ over ocean and $0.05 \pm 0.15\tau$ over dark land surfaces [*Levy et al.*, 2010; *Remer et al.*, 2005b]. Over bright surfaces, such as desert, where the standard retrieval is ineffective, we use the Collection 5.1 MODIS data and where no successful retrieval has been made over bright surfaces we use the Collection 5.1 Deep Blue retrieval (using multiple radiances including the 412 nm channel) [*Hsu et al.*, 2006]. Throughout this study we use level 3 data (daily gridded $1° \times 1°$ product). The data is screened using quality flags to remove data points with more than 80% cloud cover and a standard deviation in AOD greater than 2.5 for the level 2 data within a $1° \times 1°$ region. The number of level 2 granules within each level 3 data point is also used to weight the data when aggregating into monthly averages.

[7] The Multiangle Imaging Spectroradiometer (MISR) also flies aboard the Terra satellite but employs a different viewing geometry to the MODIS instrument, using a narrower swath (400 km) and nine camera angles. This reduces global coverage to 9 days but allows retrieval of AOD over bright surfaces, with an accuracy of $\pm 0.05 \pm 0.20\tau$ over land and better than $\pm 0.04 \pm 0.10\tau$ over ocean [*Kahn et al.*, 2010; *Martonchik et al.*, 1998; *Martonchik et al.*, 2004]. The Level 3 data product provides daily averaged AOD at $0.5° \times 0.5°$ resolution. Throughout this study we use MISR version 22 data for the 558 nm (green) channel interpolated to 550 nm for consistency with MODIS and AERONET. The data is filtered to remove level 3 pixels containing level 2 data that has a standard deviation in AOD greater than 2.5.

[8] The Cloud-Aerosol Lidar With Orthogonal Polarization (CALIOP) was launched aboard the CALIPSO satellite in 2006 as part of the A-Train constellation (local crossover at 0130 and 1330 local time). CALIOP measures vertical profiles of aerosol backscatter and extinction at 532 nm and 1064 nm in addition to total column AOD during both the night and day [*Vaughan*, 2004; *Young and Vaughan*, 2009]. CALIOP level 2, v3.01 5 km aerosol extinction retrievals are examined here for 2007. CALIOP level 2, v3.01 5 km aerosol extinction retrievals are examined here for 2007. We follow the method of B. J. Ford and C. L. Heald (An A-Train satellites and model assessment of the vertical distribution of pollution transport in the Northern Hemisphere, submitted to *Journal of Geophysical Research*, 2011) to filter the raw CALIOP data, based on extinction uncertainty and quality control flags. The cloud-aerosol-distinction (CAD) score is used to remove cases with low confidence in aerosol-cloud identification (absolute values CAD < 20), and we consider only clear-sky extinction retrievals.

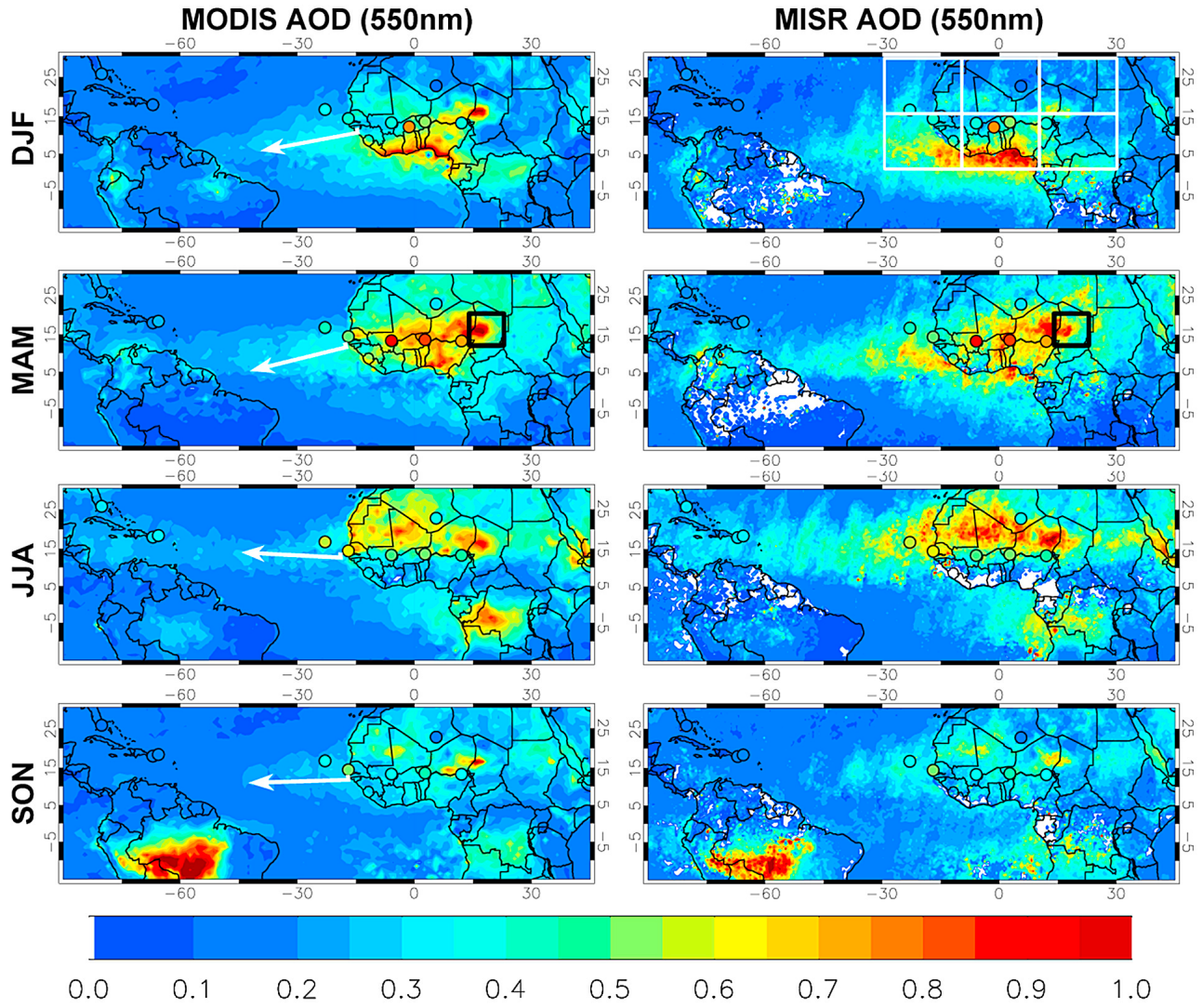

Figure 1. Seasonal maps of aerosol optical depth (AOD) for (left) Moderate Resolution Imaging Spectroradiometer (MODIS) and (right) Multiangle Imaging Spectroradiometer (MISR) are shown for 2007 in their respective resolutions of 1° by 1° and 0.5° by 0.5°. The rows from top to bottom correspond to winter, spring, summer, and fall seasons. AOD observed at African Aerosol Robotic Network (AERONET) stations used in this study are plotted as solid circles. All available AERONET data are used for each season, and only stations with over 10 days of available data in the season are displayed. The white boxes in the MISR DJF plot show the regions used in Figure 2, the black box in the MAM season highlights the Bodélé dust source region, and arrows indicate the direction of dust outflow.

2.2. Spatial Distribution of African Dust

[9] We characterize dust loading over Northern Africa and export across the Atlantic using several different observational platforms. We add to previous dust climatology studies [*Christopher et al.*, 2011; *Huang et al.*, 2010] by examining AOD observations from both MISR and the latest MODIS Deep Blue retrievals over bright surfaces, along with AERONET ground station measurements. The seasonal and regional loading of dust over Africa is investigated, developing an observational baseline against which model simulations of export of dust from Africa can be evaluated.

[10] Figure 1 shows the seasonal aerosol optical depth over Africa and its outflow region retrieved by MISR and MODIS (sampled coincidentally at 1° × 1° resolution) for 2007. The seasonally averaged AOD retrieved from AERONET stations are also displayed as circles. The variation in dust source with season over North Africa is clear in both sets of observations. These can be characterized as follows: (1) a constant emission source from the Bodélé region peaking during the spring season, (2) a maximum in west coast Sahara emissions during the summer season, (3) high coastal AOD dominating the winter season, and (4) relatively low emissions during the fall season. The Bodélé region (centered in Chad at 17°N, 18°E, highlighted with a black rectangle in Figure 1) is a constant source of dust throughout the year and is suggested to influence the AOD over much of West Africa [*Schepanski et al.*, 2009a]. Recent studies have investigated the importance of this

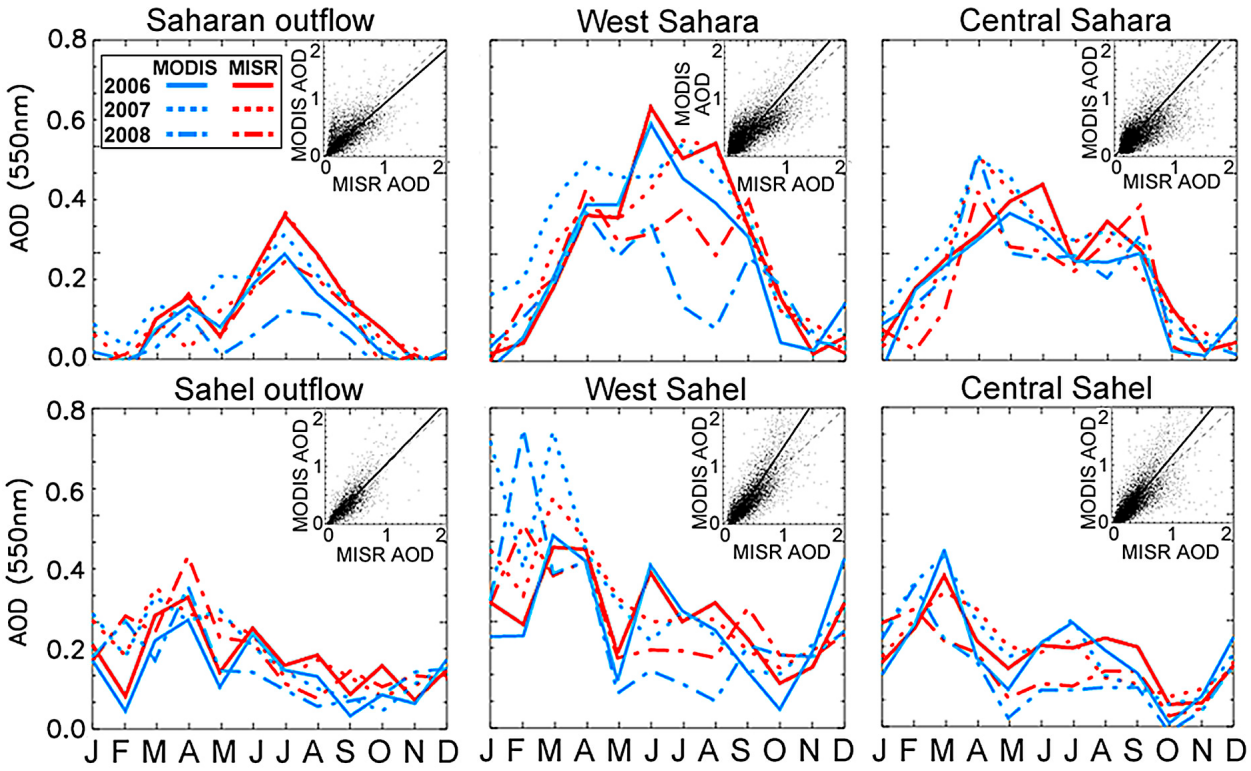

Figure 2. AOD retrieved by MODIS (blue lines) and MISR (red lines) for the period 2006–2008. Each year is displayed with a different line style (2006, solid; 2007, dashed; 2008, dash-dotted). Each of the regions corresponds to a 20° × 15° region between 0°–30°N and 30°W–30°E (shown in white in Figure 1), and regions are arranged in geographical order.

region as a source of mineral dust aerosol involved in long-range transport to the Amazon [*Ben-Ami et al.*, 2010; *Bristow et al.*, 2010; *Tegen et al.*, 2006] with estimates of up to 50% of all dust arriving in the Amazon coming from this region [*Koren et al.*, 2006].

[11] During the summer months the majority of long-range dust transport is toward the Caribbean, while in winter and spring seasons, the southward shift of the ITCZ directs more dust toward South America. This transport can be seen in the seasonal AOD shown in Figure 1 and is indicated with arrows.

[12] Aerosol is prominent over the Western Sahara in both the MISR and MODIS observations during summer months, with the seasonal average AOD generally higher for MISR than MODIS (between 0.6 and 0.9 for MISR and between 0.5 and 0.8 for MODIS). Unfortunately, there are very few surface observations in this region to verify the intensity of the AOD observed by these two platforms.

[13] The AOD over the Sahel region during the winter results from biomass burning [*van der Werf et al.*, 2003] with some contribution from upwind dust sources likely. A discontinuity in AOD is observed in the coastal region for MISR during the winter, with higher AOD over the ocean than the land. This discontinuity is present in MODIS however it is reversed. The retrieval method changes between land and ocean for both instruments and has previously been shown to result in discontinuities [*Levy et al.*, 2005]. An increase in at coastal regions AOD has been observed in MISR previously, and is possibly a result of sediments in coastal regions increasing the albedo of the ocean and hence affecting the aerosol retrieval [*Di Girolamo et al.*, 2004; *Martonchik et al.*, 2002].

[14] The majority of AERONET sites are situated at the northern border of the Sahel region where the seasonally averaged ground station measurements of AOD agree well with both MISR and MODIS (see Figure 3). Further north, the limited AERONET data available from the Tamanrasset station indicates that the satellite observations may slightly overestimate the AOD in the Sahara. Comparisons by *Kalashnikova et al.* [2011] over bright-surfaced regions of China suggest that MISR agrees better with surface observations than MODIS, however that does not seem to be the case over Africa indicating that differences may be region specific based on the limited observations available.

2.3. Seasonal Variability in African Dust

[15] Figure 2 shows the monthly mean AOD from MISR and MODIS averaged over different regions influenced by African dust for each of 3 years (outlined in white on the MISR DJF plot in Figure 1). The regressions between MISR and MODIS for daily observations over the study period are also shown for each of the regions. In both sets of observations the seasonality in AOD can be seen to follow a distinctly different pattern above and below 15°N. In the Sahel region (below 15°N) biomass burning occurs during boreal winter (December to February, DJF) whereas the burning takes place further south during boreal summer (June to August, JJA). In the winter dust is carried across the Sahel

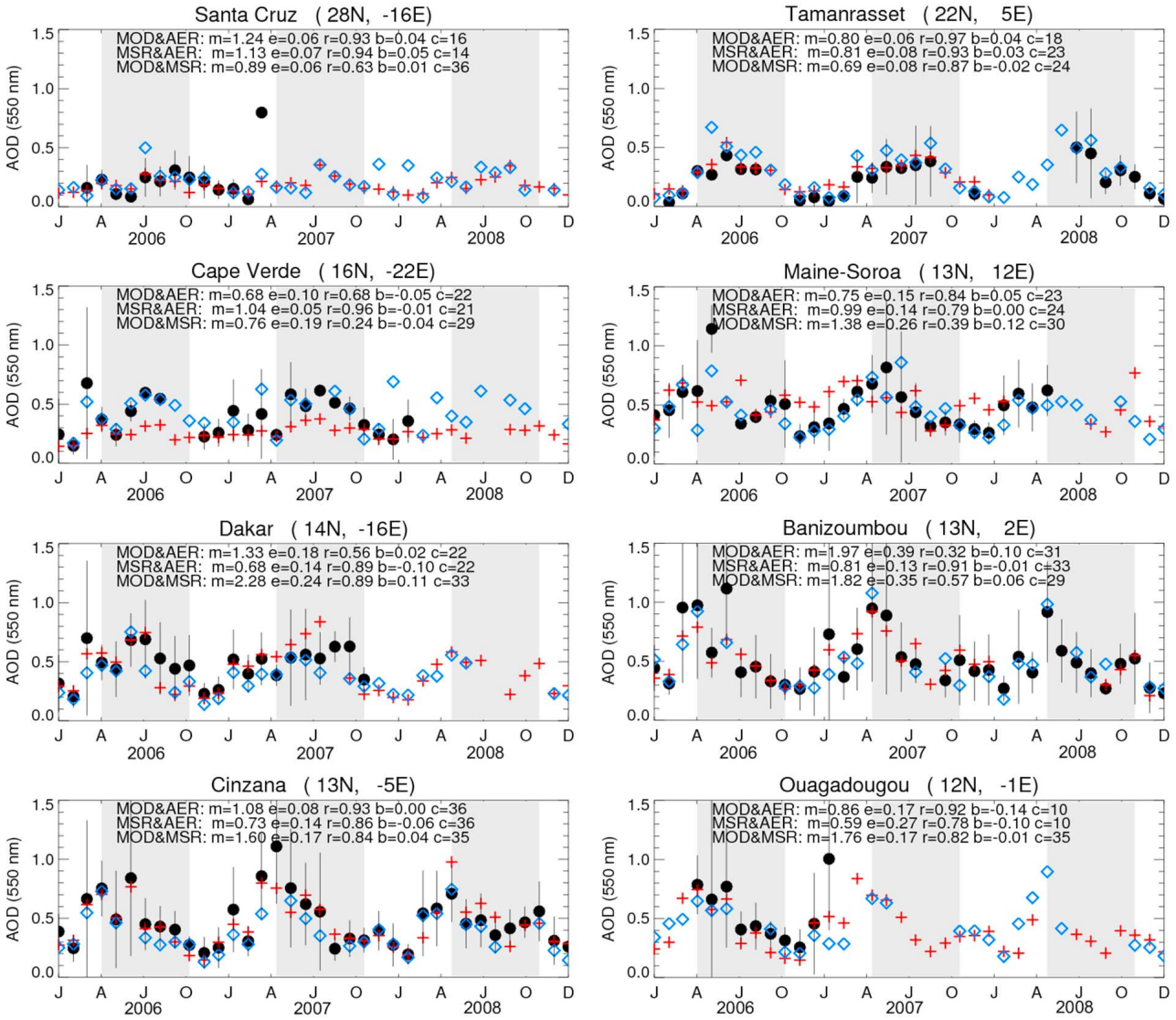

Figure 3. Time series of AOD observations from AERONET (solid circles, AER), MODIS (red crosses, MOD), and MISR (blue diamonds, MSR) for 2006–2008 are shown at the eight AERONET sites. Shaded regions indicate the summer period. Monthly averages calculated from daily data are shown with error bars indicating the standard deviation of data within each month. All available data for each platform are shown to maximize data and illustrate climatology (rather than a cross-comparison of observations). The gradient (m), RMS error (e), correlation coefficient (r), bias (b), and number of months used (c) are shown for comparison between each of the observation platforms. Matched daily data are used for these statistics.

region toward the equator as a result of the southerly position of the ITCZ. The high AOD observed during boreal winter in the Sahel region is therefore a combination of both dust and biomass aerosol. Later in the year the AOD is primarily a result of dust as biomass burning moves southward. The minimum AOD generally occurs during September to November (SON) when biomass burning is absent and dust export occurs further north. At latitudes higher than approximately 15°N the AOD has a clear peak during summer as a result of Saharan dust emissions. The AOD in boreal winter is relatively low in this region resulting from the combination of dust transport to lower latitudes, weaker dust emissions from northwest African regions, and very little contribution from biomass aerosols.

[16] MODIS and MISR retrievals in the Sahel and Sahara agree in terms of the correlation (r) of seasonality within each region ($r > 0.7$ for all regions). There is a significant bias (b) toward higher AOD in the MISR observations relative to MODIS during the JJA period ($b > 0.05$) primarily in the Saharan region and the related outflow. MODIS is biased high during the DJF season in the Sahel region ($b > 0.05$) however the bias is not apparent in the outflow region.

[17] Figure 3 shows the time series of AOD observations at these sites for AERONET, MODIS and MISR (sites used are shown in Figure 1). AERONET observations between 0930 and 1130 LT are used to produce the monthly average AOD as to coincide with the MISR and MODIS Terra

overpass. We are interested in the climatology of the dust, therefore all available data for each instrument is displayed in Figure 3 (sampling to days when all data is available reduces the data set to 13% of the total data and often does not represent the monthly average well). However, the mean (m), RMS error (e), correlation (r), and bias (b) statistics shown are calculated using days when data is available from all instrument compared. The bars on the AERONET observations (circles) indicate the standard deviation of the daily AOD within the monthly average. The majority of the AERONET sites lie just south of 15°N, and there is a clear seasonal cycle at many of these sites (Banizoumbou, Cinzana, Maine-Soroa) with peak in AOD in spring and a minima in Fall, in agreement with the broader results displayed in Figure 2. The most northern sites (Tamanrasset, Dakar and Cape Verde) show a peak in AOD during the summer rather than spring, and minima in the winter. The observations indicate that the monthly average AOD is often between 0.5 and 1.0 during dusty periods, and the AOD rarely dropping below 0.2, except in the winter months at the northernmost Tamanrasset and Santa Cruz sites.

[18] Both MISR and MODIS AOD show good agreement with AERONET for the majority of sites ($r > 0.8$ at six and five stations, respectively) and although there are considerable differences in AOD between observations for individual months (e.g., Dakar and Ouagadougou) there is no consistent bias across the stations or instruments. Considering the winter and spring seasons (when biomass burning occurs) separate from summer and fall does not significantly alter the agreement between AERONET and the MISR at these locations. However, agreement between MODIS and AERONET does show a weak seasonal dependence at the Cape Verde, Maine-Soroa and Dakar sites. This may suggest that the differences in seasonality between MISR and MODIS in the Sahel region (displayed in Figure 2) are more likely to be a result of the MODIS retrieval, however more extensive surface observations over the region would be needed to confirm this.

[19] In Figures 1–3 there are differences between MODIS and MISR retrieved optical depths. The MODIS Deep Blue retrieval generally shows lower AOD values than the MISR retrieval, especially over the Saharan dust source regions. There appears to be a seasonal bias in this, with poorest agreement during summer and fall months (Figure 2) when the MODIS AOD can be up to 30% lower than MISR AOD. These biases are broadly consistent for the 3 year period of this study (2006–2008). Previous studies have shown good agreement between MISR and MODIS, using level 2 data for colocated retrievals over ocean [*Kahn et al.*, 2007, 2011] but have also highlighted areas such as the Sahel where agreement can be poor due to the combination of dust and biomass aerosol [*Kahn et al.*, 2009]. We find that the AOD estimates from these instruments diverge when based on cosampled global gridded level 3 data and over bright surfaces, requiring the Deep Blue retrieval method. In this study the MODIS data has been weighted so that days with more level 2 data in the level 3 grid box averages are more significant. When this weighting is removed the results are similar, indicating that weighting is not a source of the bias. The MODIS and MISR AOD retrievals are independent and based on different radiance measurements (wavelengths and/or viewing geometry) with retrievals incorporating atmospheric and surface characteristics as well as assumptions about particle type and optical properties. A possible explanation for the differences in the AOD retrieval is that the surface reflectance assumptions may differ significantly between the two retrievals over the bright Saharan desert where the reflectance has a stronger impact on the AOD retrieval for both MISR and MODIS [*Kahn et al.*, 2009]. However, the bias is not limited to land observations with MISR showing higher AOD in the Saharan outflow region also (Figure 2, top left), suggesting that land surface reflectance assumptions made by the retrievals cannot fully explain the difference. These differences in AOD present a challenge for model evaluation. We will use observations to evaluate a dust simulation in this study, therefore we compare with AERONET, our "ground truth," where available and also take into account the range of the satellite-retrieved observations of AOD.

2.4. Interannual Variability of African Dust

[20] Although there is considerable seasonal variability in the AOD we find that the seasonality is largely consistent from year to year over the period 2006–2008. AOD is highly spatially correlated ($r > 0.8$) from year to year for all seasons over the region shown in Figure 1. The interannual variation in AOD for the same region is generally less than 30% seasonally. From Figure 2, most interannual variability occurs during the winter season which is likely to be a consequence of the occurrence of both dust and biomass burning episodic events. Where possible we use all 3 years of data in analysis, however, as the interannual variability is relatively small we assume it is reasonable to draw conclusions from single year comparisons throughout this study.

2.5. Diurnal Variability in African Dust

[21] To investigate the diurnal variability in the observations we have used hourly AERONET data alongside the two MODIS instruments. Diurnal variability in dust close to sources in North Africa is well documented in several studies [*Eck et al.*, 2003; *Mbourou et al.*, 1997] with a peak in dust emission during the morning based on satellite retrievals [*Schepanski et al.*, 2009b]. *Smirnov et al.* [2002] were unable to find a significant diurnal cycle in AOD for a group of dust-influenced AERONET sites; however, these were located at regions across the globe. We use the observations to investigate whether this diurnal variability impacts the column AOD at several AERONET sites influenced by African dust. The Deep Blue retrieval is available for the MODIS instrument aboard both the Terra and Aqua satellites that make an equatorial overpass at 1030 and 1330 local time, respectively. Hourly measurements from AERONET stations have been used to create an average AOD for morning (0930–1130) and afternoon (1330–1530) periods We find that very few individual months show significant differences between the morning and afternoon AOD in either the AERONET or MODIS observations. Analyzing summer and winter independently (to account for biomass burning influence during the first months of the year) shows no difference over the 3 year period. The only site that shows a possible consistent diurnal cycle is the Tamanrasset site located furthest north, with a tendency toward higher AOD in the afternoon (mean differences of -0.03, and -0.04 for AERONET and MODIS, respectively). This occurs April to

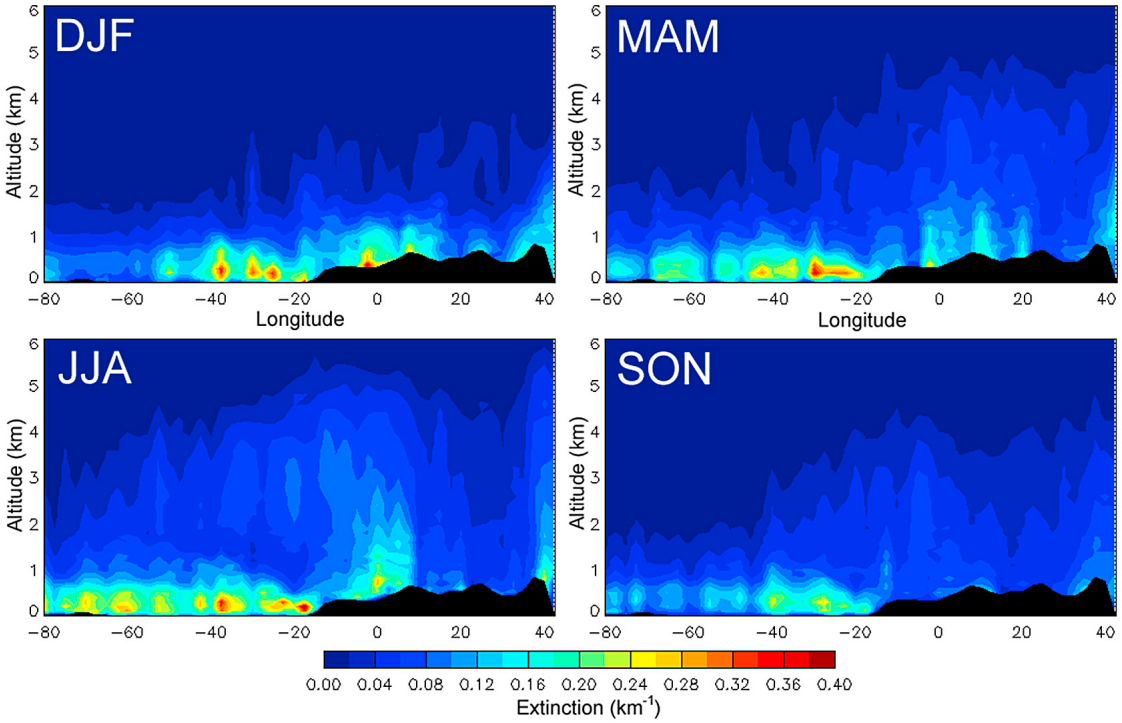

Figure 4. Cloud-Aerosol Lidar With Orthogonal Polarization (CALIOP) retrievals of aerosol extinction are shown as curtain plots from 80°W to 40°E for each season of 2007. Data are averaged in 5° longitudinal bands between 10°N and 25°N for all seasons except MAM, when the transect is skewed from 10°–25°N to 0°N–15°N from east to west to account for the prevailing wind direction. The black regions indicate landmass.

July, however there is not enough data to show this to be significant. This indicates that, although day-to-day diurnal variability in dust emissions has been observed, on average there is no consistent difference in the AOD at these AERONET sites for the overpass times of the Terra and Aqua satellites. We therefore conclude that differences between MISR and MODIS-Aqua observed AOD represents retrieval and instruments differences rather than diurnal variation in dust.

2.6. Vertical Distribution of Dust Aerosol

[22] Figure 4 shows curtain plots of aerosol extinction along a longitudinal transect from CALIOP. The data is averaged over regions of 2.5° longitude between 80°W and 40°E, and over latitudes of 10°–25°N for four seasons. The black region indicates the land relief of the African continent.

[23] There appear to be two regions of enhanced aerosol in the observations – one close to the surface over the Atlantic, and one that begins high over the African continent and descends as it moves west. The low-altitude feature exhibits relatively high extinctions that are determined to be a mixture of marine aerosol and dust in the CALIOP retrieval. The second feature aloft shows strong seasonality with dust ascending to 4–5 km during spring and summer, and generally staying below 2 km in the fall and winter months. In the outflow, the dust can be seen to descend more rapidly in the spring than in summer as it crosses the Atlantic. Although the averaging and sampling methodology used differs from *Huang et al.* [2010] we find similar plume heights and rate of descent during transport for both winter and summer.

3. Simulating Dust in the GEOS-Chem Model

3.1. Model Description

[24] The GEOS-Chem model (version v8-03-01; http://www.geos-chem.org/) has been used to conduct a global three-dimensional simulation of coupled oxidant-aerosol chemistry over the period 2006 to 2008 at a resolution of 2° × 2.5° latitude and longitude, and 47 vertical levels. The model is driven by assimilated meteorology from the Goddard Earth Observing System (GEOS-5) of the NASA Global Modeling and Assimilation Office (GMAO), which includes assimilated meteorological fields at 3-hourly and 6-hourly temporal resolution. The aerosol types simulated include mineral dust [*Fairlie et al.*, 2007; *Zender et al.*, 2003a], sea salt [*Alexander et al.*, 2005], sulfate-nitrate-ammonium aerosols [*Park et al.*, 2004], and carbonaceous aerosols [*Henze et al.*, 2008; *Liao et al.*, 2007; *Park et al.*, 2003].

[25] Aerosol optical thickness (AOT) at 550 nm is calculated online assuming lognormal size distributions of externally mixed aerosols and are a function of the local relative humidity to account for hygroscopic growth [*Martin et al.*, 2003]. Aerosol optical properties employed here are based on the Global Aerosol Data Set (GADS) [*Kopke et al.*, 1997] with modifications to the size distribution based on field observations [*Drury et al.*, 2010; *Jaeglé et al.*, 2010].

Table 1. Proportion of Dust Mass Observed During Different Campaigns Shown at the Radii of the Four GEOS-Chem Dust Mass Sizes[a]

	Proportion (%)			
Mean Radius (um)	*Haywood et al.* [2003a, Figure 6]	*Highwood et al.* [2003, Figure 4a]	*Highwood et al.* [2003, Figure 4b]	*Osborne et al.* [2008, Figure 10]
0.15	2	12	**6**	10
0.25	13	8	**12**	13
0.40	20	24	**24**	27
0.80	65	56	**58**	50

[a]The normalized fractions of dV/dlnR as shown in the original figures are displayed along with the corresponding percentages. The values shown in bold are those used in the updated GEOS-Chem model. The first column values are from a lognormal fit to passive cavity aerosol spectrometer probe data during the Saharan Dust Experiment campaign [*Haywood et al.*, 2003a]. The *Highwood et al*. [2003] values are from differing Sun photometer retrievals, their Figure 4b values being used throughout the work of *Highwood et al.* [2003], and the *Osborne et al*. [2008] values are from BAe-146 measurements during the DABEX campaign.

[26] The DEAD dust scheme is used in the model for calculation of source and emission of dust aerosol [*Zender et al.*, 2003a]. We note that *Fairlie et al.* [2007] found better agreement with observations in the United States when combining the GOCART scheme dust sources with the DEAD emission scheme in GEOS-Chem. However, the issues raised by *Fairlie et al.* [2007] regarding the leaf area index (LAI) used in the DEAD source function (which caused too high dust emission over the U.S. plains) are less applicable to production of dust from desert regions. In the DEAD dust scheme the kinematic and thermodynamic properties of the boundary layer are determined by assuming that the surface and atmosphere maintain thermal equilibrium with the radiation field by constantly adjusting surface heat, vapor, and momentum exchanges [*Bonan*, 1996]. This allows for the surface wind friction speed to be modeled which leads to saltation (horizontal dust flux). The saltation process is dependent upon the wind exceeding a critical threshold that is determined by soil type, moisture content, and surface roughness. Dust particles are emitted in four size ranges (0.1–1.0, 1.0–1.8, 1.8–3.0, and 3.0–6.0 μm radius) based on observations [*d'Almeida*, 1986; *Schulz et al.*, 1998]. The total amount of dust emitted is tuned in GEOS-Chem to give a global dust emission around 1500 Tg yr^{-1}. The submicron dust is carried as a single tracer resulting in limited size distribution information for the fine dust aerosol. While differences in sedimentation may be small for submicron aerosol, differences in light scattering efficiency in the visible (400–700 nm) are not. Therefore the smallest size bin is converted into four size bins when assessing the light scattering properties.

[27] Within the model aerosol is removed by both wet and dry deposition. Dry deposition occurs primarily though gravitational settling and is inefficient for aerosol smaller than 2 μm in diameter. Therefore dry deposition is most important close to source, especially for dust, and removal downwind is dominated by wet processes. These processes involve rainout (nucleation scavenging when water condenses onto the aerosol), washout (impaction scavenging by raindrops) and convective removal [*Liu et al.*, 2001]. In the GEOS-Chem model, convective removal accounts for subgrid-scale precipitation events by removing a fraction of the aerosol in convective updrafts. If this subgrid-scale process is not accounted for then the aerosol is lofted into the upper troposphere and advected at high altitude [*Jacob*, 2000].

3.2. The Impact of Dust Mass Partitioning on the AOD

[28] In the standard GEOS-Chem model, the dust mass in the smallest of the four dust tracers in is partitioned equally into four submicron size bins (with radii centered at 0.15, 0.25, 0.4 and 0.8 μm) used for the optical calculation. However, this is not physically realistic when compared to in situ measurements of African dust during the SAFARI and DABEX campaigns [*Haywood et al.*, 2003a; *Highwood et al.*, 2003; *Osborne et al.*, 2008]. These observations show that the mass is concentrated at larger sizes, rather than equally distributed. Table 1 shows the partitioning of submicron dust mass at different sizes based on three different observational campaigns. The results are relatively consistent between measurements, showing that mass is concentrated at the larger aerosol sizes, with only 5%–10% in the smallest size range, considerably less than the 25% previously assumed in the model. We modify the dust mass partitioning in GEOS-Chem to match the fractions documented in the work of *Highwood et al.* [2003, Figure 4b]. These data are used as they are selected for use by *Highwood et al.* [2003] and also lie within the range of the other observations for each aerosol size in Table 1. It should be noted that the change in size distribution only applies to the calculation of dust optical properties, hence there is no change in the dust aerosol mass within the simulation.

[29] Figure 5 displays the annually averaged difference in AOD from the change in mass partitioning over the African dust source and export region. The more realistic partitioning results in a lower AOD in all locations, especially near source where the dust AOD is highest. Near source the AOD is reduced by up to 0.3 resulting in a 25% decrease. As the model has previously been shown to overestimate dust AOD close to source [*Generoso et al.*, 2008] this improves agreement with observations (see discussion in section 3.3). The reduction downwind can be as high as 40%, a result of a larger fraction of the AOD being due to submicron aerosol as the larger dust sediments out. The boxes in Figure 5 (top) show the AOD contribution (at 550 nm) from each of the seven dust aerosol optical size bins at locations along the common transport pathway from North Africa for both new and original versions of dust partitioning (red and blue bars, respectively). At 550 nm the light scattering efficiency per unit mass is greatest for the smallest submicron dust aerosol considered in the model. With the new

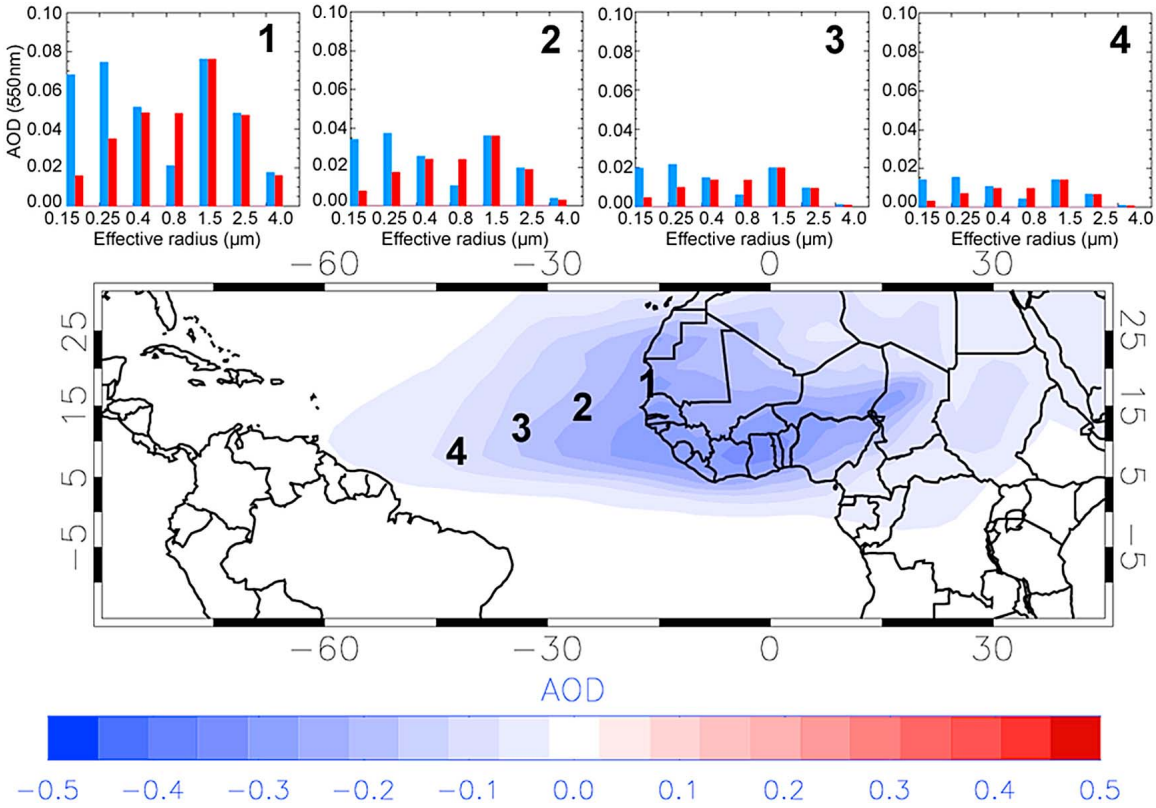

Figure 5. (bottom) The difference in annual mean AOD (at 550 nm) resulting from altering the partitioning of dust mass in the submicron sizes when calculating the optics is shown between 30°N and 20°S. (top) The AOD contribution from each of the size bins is shown for both new (red lines) and original (blue lines) dust partitioning for four locations across the African dust outflow. The locations of the size distributions are numbered on the map of AOD difference.

partitioning, mass at these sizes has been shifted to larger sizes and therefore results in a reduction of the total AOD.

3.3. Comparison of GEOS-Chem AOD With MODIS, MISR, and AERONET

[30] Figure 6 compares the AOD for MISR, MODIS, with both the new submicron dust partitioning and baseline versions of the model over Africa and the outflow to the Americas. The model has been sampled to only use days and locations when both MODIS and MISR are available. Comparison with MODIS and MISR observations of AOD show that better agreement is achieved over the majority of North Africa in terms of the gradient with the new submicron partitioning (based on the data within the entire boxed region on Figure 1). There is no significant change in the spatial correlation between the model and observations as the impact of changing the dust size partitioning is a general decrease in AOD. The AOD far from source was previously underestimated with respect to MODIS observations. The reduction in AOD due to the improved dust mass partitioning now makes this more apparent. As the magnitude of the GEOS-Chem AOD generally agrees better with the observations at source this would suggest that transport or removal processes are responsible for this discrepancy. These processes are investigated in section 4.

[31] Figure 7 compares time series of AOD from both GEOS-Chem dust partitioning settings with monthly AOD from AERONET, MODIS and MISR. Using the new partitioning reduces the RMS error between modeled and observed AOD at all the eight AERONET sites affected strongly by African dust, and the gradient is also closer to unity at all but the Cape Verde site. With the new submicron dust partitioning the AOD is generally biased slightly lower in GEOS-Chem relative to AERONET in contrast to previous versions of the model overestimating AOD over North Africa [*Generoso et al.*, 2008]. Both the spatial and seasonal variability of AOD are generally well captured over North Africa and in the Atlantic outflow and the regions with high seasonal AOD are broadly consistent between model and observations. Emissions from the Bodélé depression are evident, although somewhat lower than observations suggest. Considerable differences are apparent between simulated and observed AOD in central Africa but these are due to differences in biomass burning, not dust. This biomass burning discrepancy is not model specific and has been documented by *Giglio et al.* [2003].

[32] There appears to be a consistent missing source of dust between July and September when the model underestimates the AOD each year at several sites (Figure 7). This is at a time when biomass burning moves further south toward Central Africa, therefore it is unlikely that biomass emissions can explain the higher AOD seen in all the observational data sets. Figure 6 shows that the model substantially underestimates the emissions from the Bodélé

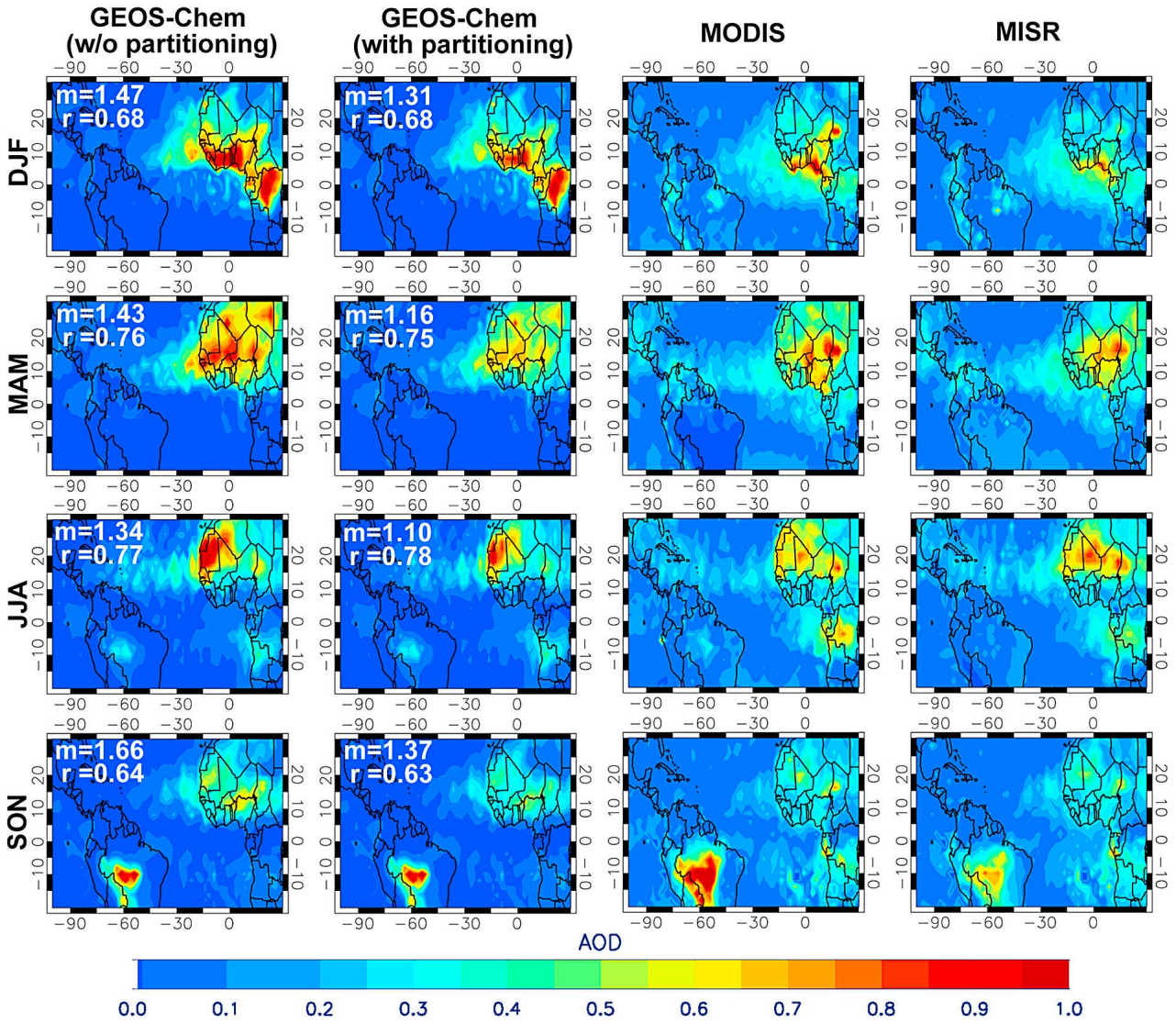

Figure 6. Seasonal AOD for original GEOS-Chem, GEOS-Chem with new dust partitioning, MODIS, and MISR are shown over the African outflow region. All data are gridded on the model 2° by 2.5° resolution. The gradient (m) and correlation coefficient (r) are shown for comparison between the GEOS-Chem and MODIS.

region at this time, therefore this may contribute to the poor agreement at measurement sites downwind. Increasing the emissions from the Bodélé region by a factor of two improves agreement with MISR and MODIS over the North African region. The spatial correlation is improved by 5%–10% and the RMS error reduced by 30% for all seasons. Any further increase in emissions degrades the agreement with satellite observations as a result of excessive AOD downwind of the Bodélé region. This indicates that the meteorological fields may not be sufficiently high resolution to represent the high wind speeds encountered between the mountain ranges in this relatively small region [*Washington and Todd*, 2005].

[33] The AOD resulting from the dust plume traveling westward across the Atlantic appears to decrease more rapidly in the model than in the observations (Figure 6). This is partly the result of the background AOD being lower in the model. The AOD over unpolluted regions of the ocean is approximately 0.05 lower than MODIS and MISR. Although cloud screening and other averaging techniques can impact this, there may be missing sources of fine marine aerosols in the model [*Jaeglé et al.*, 2010; *Lapina et al.*, 2011]. Taking the background AOD bias into account it appears the decrease in AOD westward still occurs more rapidly in the model than observations, suggesting that removal may be too rapid.

[34] The model consistently shows lower AOD than observed off the coast of Africa below 5°N throughout all seasons. There is often a sharp latitudinal gradient in the AOD (e.g., DJF season in Figure 6) that is not apparent in the observations. The Intertropical Convergence Zone (ITCZ) is relatively stationary over West Africa and is a region associated with strong convection and high precipitation. This region shows cloud cover >75% based on the

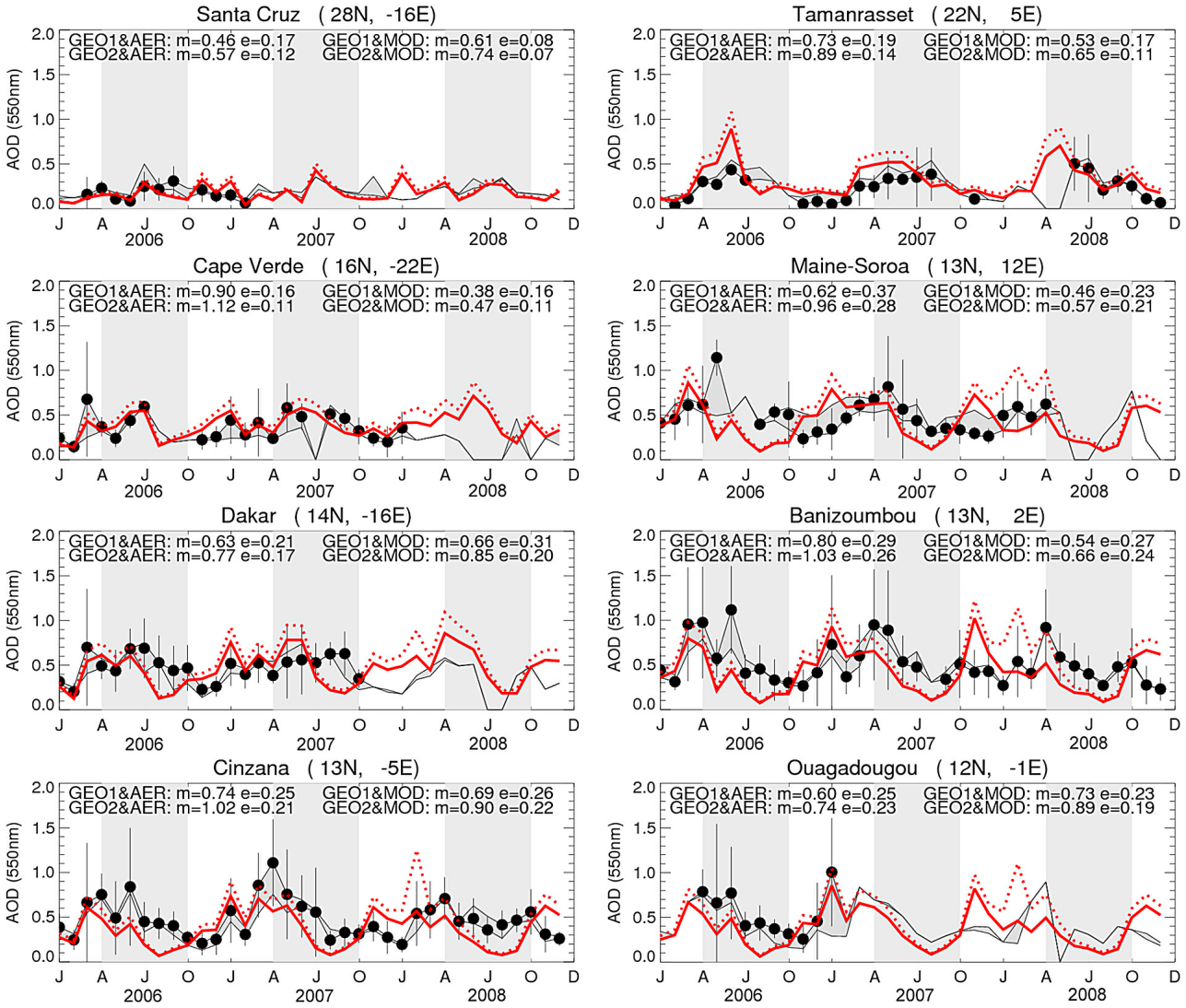

Figure 7. Monthly AOD (at 550 nm) at the eight AERONET sites is shown for the 2006–2008 period. Versions of GEOS-Chem with new submicron partitioning (GEO2, solid red line) and original partitioning (GEO1, dotted red line) are shown along with AERONET (circles) and the range of AOD from the observations including AERONET, MODIS Terra, and MISR (shaded envelope). GEOS-Chem is sampled to only use days when AERONET and MODIS data are available (if no observations are available for the month, then all days are used in the GEOS-Chem average). The gradient (m) and RMS error (e) between GEOS-Chem with new and old partitioning (GEO2 and GEO1, respectively) and the AERONET (AER) and MODIS Terra (MOD) observations are shown in the inset. Shaded regions indicate summer season.

ISCCP cloud cover data (http://isccp.giss.nasa.gov/) and at this location the dominant removal mechanism in the model is found to be through convective updrafts. The removal of aerosol via wet processes is known to entail considerable uncertainty [*Alheit et al.*, 1990; *Croft et al.*, 2010; *Flossmann and Pruppacher*, 1989; *Zhao and Zheng*, 2006].

[35] To assess removal processes previous studies have compared model results with measurements of metal deposition, and inorganic aerosol wet deposition from sites around the globe and found reasonable agreement [*Fisher et al.*, 2011; *Liu et al.*, 2001]. However, these are primarily based over continental regions. We have used MODIS AOD observations to indicate whether the model is capturing the removal of aerosols as they are carried across the Atlantic. The reduction in optical depth has been calculated along transects from the coast of Africa out toward America (approximately 20°W to 60°W) for both MODIS and for the model. An approximate lifetime for the dust is calculated by removing the background AOD (by taking the minimum AOD over the midatlantic) so that only the dust plume is considered. Wind fields indicate easterly wind speeds of approximately 10 m s^{-1} for the location and altitude of the dust plumes (taking the seasonal variation of plume height into account), and from this we derive the lifetime of the dust aerosol as the gradient of the logarithm of the AOD against time (Table 2). We assume that the aerosol removal is first order and therefore consider the logarithm of the optical depth when comparing the change in AOD along

Table 2. Lifetime of Dust in GEOS-Chem and MODIS for Each Season in 2006–2008[a]

		Dust Lifetime (days)		
	Season	GEOS	MODIS	Ratio
DJF	2006	4.4	4.3	1.0
	2007	1.8	3.3	0.5
	2008	1.8	3.4	0.5
MAM	2006	2.9	7.4	0.4
	2007	3.4	6.6	0.5
	2008	2.8	6.5	0.4
JJA	2006	3.8	5.2	0.7
	2007	5.1	7.5	0.7
	2008	4.1	14.0	0.3
SON	2006	2.1	2.7	0.8
	2007	2.2	3.4	0.6
	2008	2.2	2.0	1.1

[a]Based on the reduction in aerosol optical depth across the Atlantic. The ratio of the two lifetimes is shown under Ratio.

transects. This assumption holds true for all times other than the JJA season (when the source AOD is highest) in both the model and the observations. We note that this assumes no significant change in aerosol size distribution shape, and thus scattering efficiency, across the Atlantic (this assumption is supported by the size distributions shown in Figure 5).

[36] In most seasons the dust lifetime is underestimated by 25%–50% with respect to the lifetime calculated from the observations (e.g., 3.0 versus 6.3 days in MAM, and 2.0 versus 2.7 days in SON, averaged over all years). The dust lifetimes for each season are relatively consistent from year to year, both in the model and the observations, suggesting that there is a bias toward too much removal in the model, rather than a lack of model skill.

[37] The seasonally averaged transects are shown in Figure 8 (for 2006 to 2008 combined). The modeled AOD along the transect correlates well with MODIS for all seasons, however the model shows AOD up to 50% higher at source and subsequently a steeper trend line in the modeled AOD. For all but the summer season the AOD is both higher than MODIS at source and lower than MODIS downwind, suggesting that the removal of aerosol is consistently greater along the transects in the model (see section 4.2 for a discussion of the removal processes). In spring, the poorest agreement between modeled and observed dust lifetimes is seen which will have implications for simulating deposition to the Amazon as the majority of dust from Africa arrives during this season [*Koren et al.*, 2006]. This is discussed in section 5.

3.4. Vertical Structure of Dust Aerosol

[38] African dust emissions are often lofted high into the atmosphere in convective updrafts. This can affect the long-range transport as dust plumes at different altitudes will be subject to different dry and wet removal. To determine how well the vertical distribution of dust is captured in the model we compare with extinction profiles derived from CALIOP measurements.

[39] Previous studies have used CALIOP to evaluate the vertical distribution of modeled aerosol on a case by case basis [*Di Pierro et al.*, 2011; *Eguchi et al.*, 2009; *Generoso et al.*, 2008]. *Generoso et al.* [2008] show that in GEOS-Chem, for the two episodes they consider, the transatlantic dust plume descends slightly more rapidly in the summer than observed, and slightly slower in the winter.

[40] In this study we compare extinction profiles and outflow plume heights averaged over seasonal time scales determined from CALIOP and GEOS-Chem over the Atlantic Ocean. The purpose is to see if discrepancies in AOD between the model and observations can be attributed to the simulated plume height.

[41] The CALIOP profiles are aggregated for five 10° × 15° regions across the Atlantic (between 10°W and 60°W) for all available CALIOP data. A threshold AOD of 0.05 is set to only consider cases with significant aerosol loading and to approximate the detection limit of the CALIOP instrument. The data is averaged to produce seasonal mean profiles.

[42] Figure 9 shows the CALIOP and simulated extinction profiles averaged over the same regions for all seasons. In winter, the observed and modeled extinction profiles closest to source (red) agree well, with strong extinction at the surface and extending up to 3–4 km altitude. In the downwind region the model extinction seems to decrease slightly slower than the observations above 2 km. Below 2 km the observations show a marked increase in the extinction, and while this is captured in the model the magnitude is much reduced. Far from source (black) CALIOP shows most of the aerosol confined below 1 km whereas in the model it extends slightly higher, up to 1.5 km. In all seasons, especially during winter and spring, the extinction below 1 km over the Atlantic is considerably lower in the model than in CALIOP (identified as a mixture of marine and dust aerosol). This may be a result of excessive removal of dust at low levels in the model, as well as the missing marine aerosol source previously discussed [*Lapina et al.*, 2011].

[43] During summer, CALIOP shows elevated extinction close to sources with a peak at 3 km but extending up to

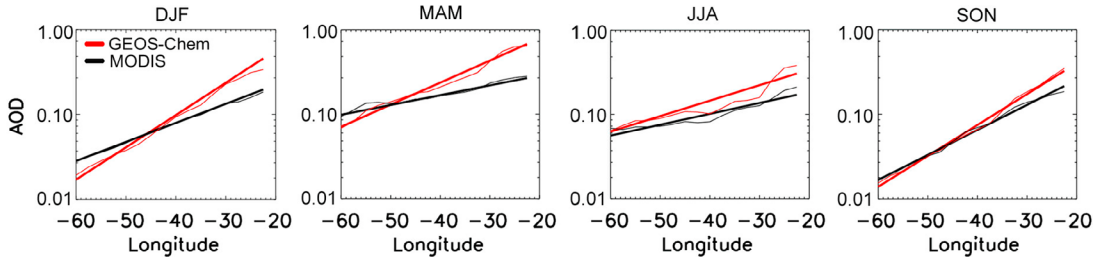

Figure 8. The seasonally averaged AOD along transects from 20°W to 60°W are shown for MODIS (solid lines) and GEOS-Chem (red lines) averaged over the 2006–2008 period. The thin lines show the average AOD along the transects, and the bold lines show the logarithmic trend line.

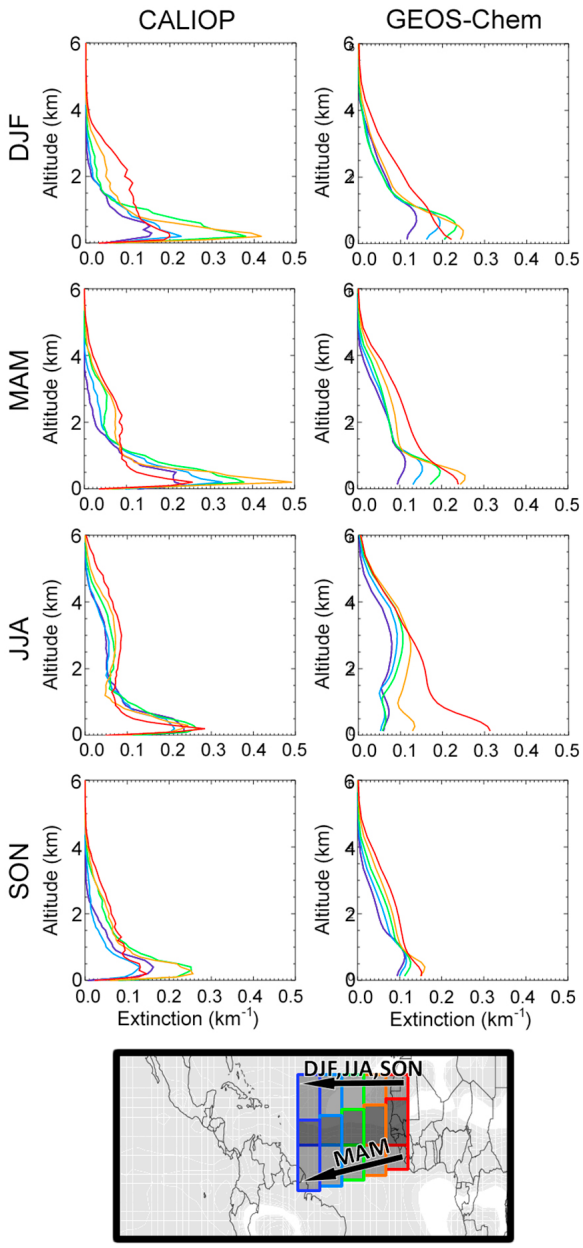

Figure 9. (top) Extinction profiles are shown for CALIOP and GEOS-Chem for each season. (bottom) The profiles are averaged over 5° by 15° regions from 0°W to 60°W (from red through to purple) and between 0°N and 25°N depending on the season, as illustrated.

6 km. In the model the plume is not quite as pronounced with a peak at 2.5 km but still extending up to close to 6 km. The extinction remains elevated in both the model and the observations as it crosses the Atlantic, however the extinction at the surface decreases more rapidly in the model.

[44] Figure 10 shows curtain plots for MAM and JJA seasons along a longitudinal transect for both CALIOP and GEOS-Chem. The data is averaged over regions of 2.5° longitude and between latitudes 10°–25°N for June through August (JJA) and averaged between latitudes 10°–25°N at 40°E descending to latitudes 5°–15°N at 80°W to account for prevailing wind direction for March through May (MAM). The model extinction is shown both when sampled to CALIOP observations and also for all available data to illustrate the departure from the seasonal mean when sampling.

[45] As described in section 2.5, there appear to be two transport pathways in the observations, one close to the surface that stays below 1 km as it moves over the Atlantic, and one that begins high over the African continent and descends as it moves west. The model is able to reproduce the vertical extent of the dust aerosol for both spring and summer, and also captures the faster descent of the dust in spring relative to summer. The low-altitude feature is less well represented, especially in summer. As in Figure 9, the observations show high extinction across much of the Atlantic where very little is present in the model.

[46] The extinction in source regions is generally higher in the model than the observations for all seasons, however the extinctions in outflow regions are comparable. This may indicate that the model produces too much aerosol at source but that it is removed quickly. The location of source regions agree reasonably well except for the summer season when they appear to be displaced east in the model relative to the observations. Comparison with MODIS and MISR showed that the model AOD was higher over West Africa during the summer than observed, which is also seen in the CALIOP comparison. However, the other differences over source indicated by CALIOP are not apparent in the comparison with MODIS and MISR. The spatial and temporal coverage of data used to generate the seasonal averages is limited due to the narrow swath of CALIOP (as can be seen by the considerable difference between the sampled and unsampled model) so the comparison between CALIOP and the model, although collocated, may not represent the full season. Because of this, and also the uncertainties inherent in retrieving extinction, we rely on MODIS and MISR to evaluate dust source regions in the model, with the additional information on outflow and transport supplied by CALIOP.

[47] On the basis of this analysis we can conclude that the model is capable of reproducing much of the aerosol vertical structure and the transport across the Atlantic, the key differences being higher extinction at dust sources and missing aerosol over the ocean that is at least partially related to dust.

4. Uncertainties in Simulating Dust Aerosol

[48] This section describes the uncertainties involved in different processes that affect dust transport in the model. This includes uncertainties arising from emissions parameterization, the vertical distribution of dust compared to observations, and wet and dry removal processes. The overall uncertainty from these aspects is determined in the context of intercontinental transport of Saharan dust.

4.1. Emission of Dust

[49] The conversion of horizontal saltating dust flux to a vertical dust flux is strongly dependent upon the soil texture [*Shao and Raupach*, 1993]. This translates to a sensitivity to the clay fraction in the model [*Zender et al.*, 2003a] with the vertical flux increasing exponentially as clay fraction increases up to 20% content. This relationship is not extended at greater clay fractions and is believed to decrease,

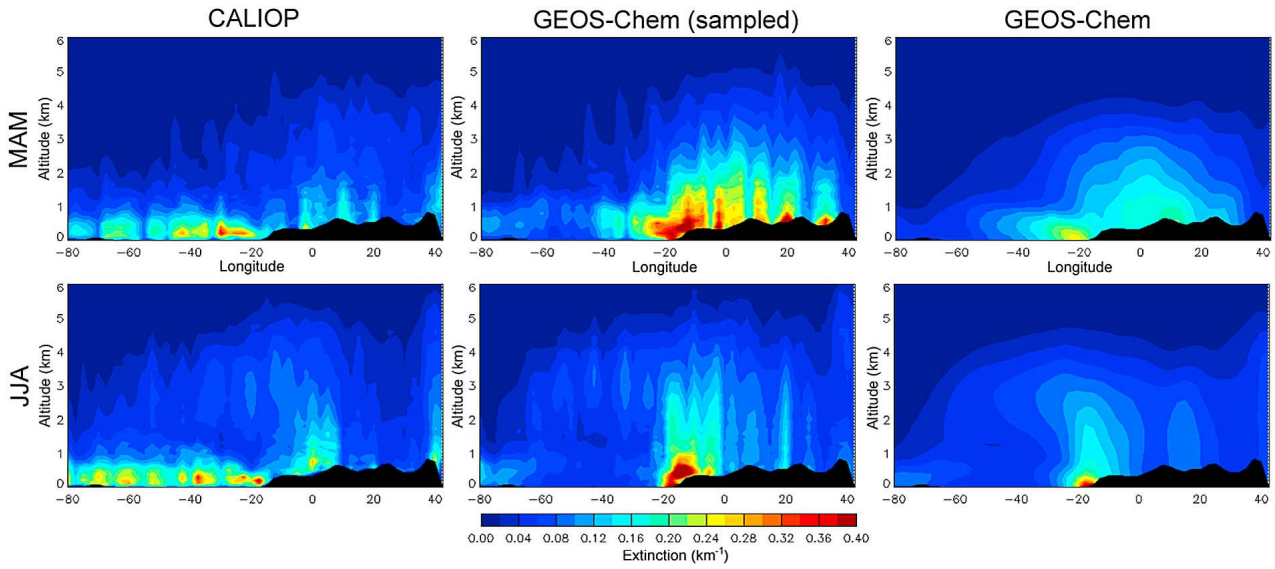

Figure 10. Seasonal extinction curtain plots for (left) CALIOP, (middle) GEOS-Chem sampled to CALIOP, and (right) unsampled GEOS-Chem are shown from 80°W to 40°E. (top) MAM and (bottom) JJA are shown. Data are averaged in 5° longitudinal bands between 10°N and 25°N for JJA season, and the transect is skewed from 10°–25°N to 0°–15°N from east to west for MAM, to account for the prevailing wind direction. The black region indicates landmass.

although little data is available [*Zender et al.*, 2003a]. Larger soil clay fractions also raise the threshold above which soil moisture can inhibit saltation [*Marticorena et al.*, 1997]. This effect is relatively small compared to that of the conversion to vertical flux which varies over 2 orders of magnitude between clay fractions of 5% and 20%.

[50] The DEAD dust scheme is sensitive to soil clay fraction, however the clay fraction has historically been kept constant globally at a value of 0.2. In reality the clay fraction varies between close to zero and 60% globally based on the IGBP soil texture data set [*Tempel et al.*, 1996]. The lowest values occur primarily in the Sahara and the Middle East with mean clay fractions over North Africa in this data set being 12% ± 5%.

[51] Figure 11 shows the difference in AOD resulting from using the IGBP soil clay fractions in the GEOS-Chem dust simulation. Using the clay fraction map reduces the annual AOD by up to 0.5 close to source in Africa, with the impact visible in dust outflow across the Atlantic and Indian Ocean. As the GEOS-Chem model tends to underestimate the AOD from dust away from source (see section 3.4) this further reduction in dust gives poor agreement with observations. However, global scaling of dust emissions in GEOS-Chem could be readjusted to compensate for this decrease. Comparison with MODIS Aqua AOD over the Sahara, the entire of North Africa, and outflow over the Atlantic all show that the correlation with monthly AOD observations is unchanged (within ±5%) when using the clay fraction map rather than the fixed clay fraction. The only exception is during the month of May when the correlation improves by 30% when comparing with both MODIS and MISR. Considering that the spatial correlation with observations is not significantly improved over Northern Africa, there is little basis for altering the sensitivity of the model to clay fraction. However, we note that the spatial variability in clay fraction is small over Northern Africa and it remains to be evaluated whether a more accurate estimate of clay fraction improves the spatial simulation of dust emissions in other regions of the world. The use of fixed clay fraction remains a source of considerable uncertainty for dust emission.

4.2. Removal Processes

[52] Figure 12 shows the relative importance of the different removal processes for dust export from Africa averaged over the entire study period Figures 12 (middle) and 12 (right). The deposition is weighted by dust mass to highlight those regions most influenced by dust. Removal via dry deposition is seen to dominate close to source and is still significant in the outflow region up to 30°W. Over the Sahel convective removal dominates while both rain out and convective removal are important far downwind in

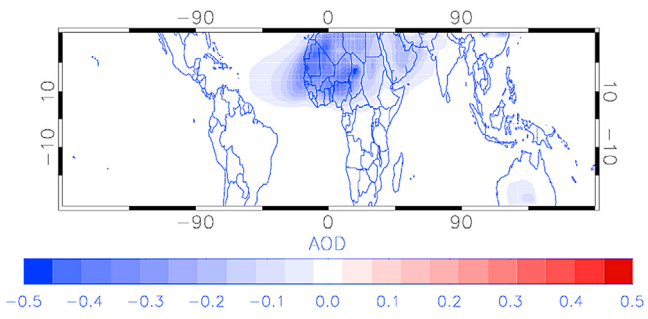

Figure 11. The impact of using the IGBP clay map (rather than a fixed fraction of 0.2) on the AOD averaged over 2006 is shown. Negative indicates a lower AOD when the clay map is used.

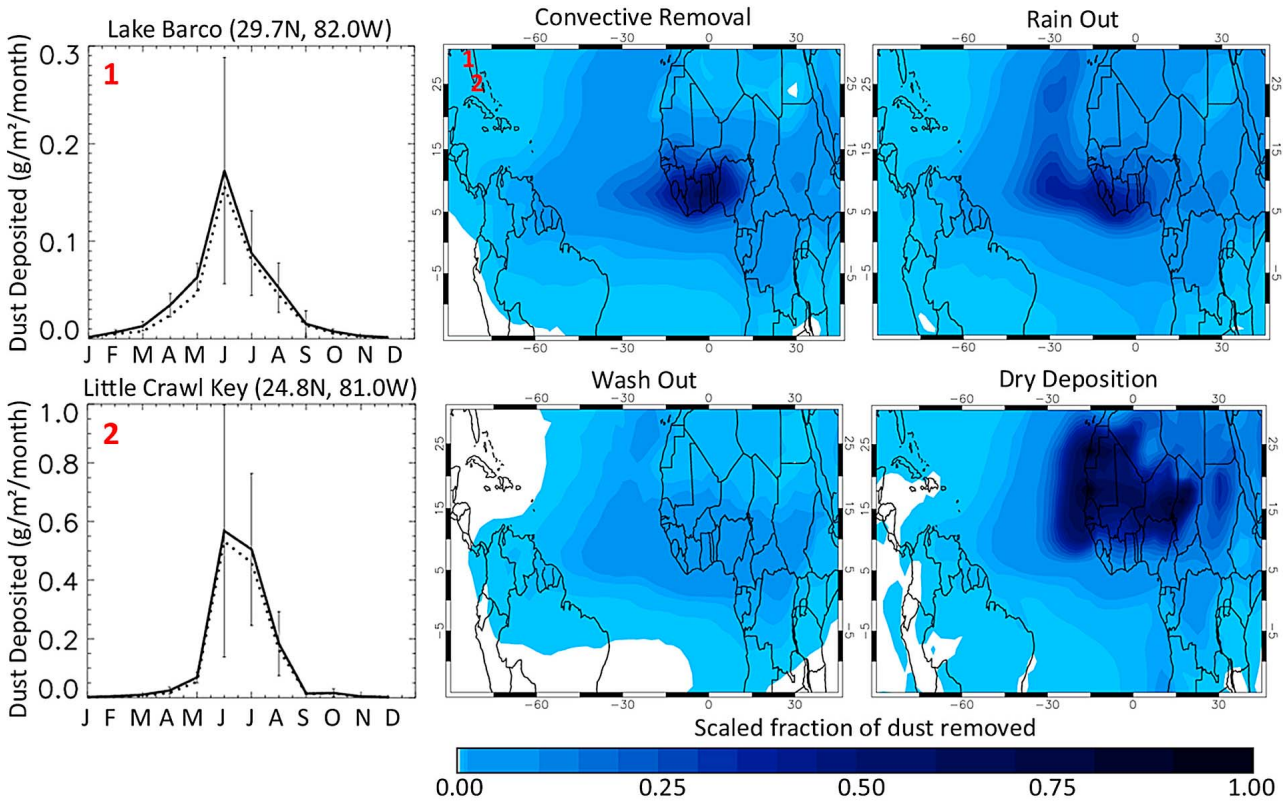

Figure 12. (right) Dust removal for the four different deposition mechanisms over Africa and in the outflow region, averaged over the 2006–2008 study period. Deposition via each process is shown as a fraction of the dust mass removed and is scaled by dust AOD to highlight the regions with most dust loading. (left) Seasonality of the modeled deposition at two measurement sites in Florida are averaged over the 2006–2008 period (numbered on the deposition plots). The total deposition (solid line) and the wet deposition (dashed line) are shown with error bars representing the interannual standard deviation.

the Americas (wash out accounts for less than 10% of the removal).

[53] *Prospero et al.* [2010] show that wet deposition accounts for more than 70% of the total annual deposition at sites across Florida from 1994 to 1996. We find that, for our model, wet deposition accounts for 84%–91% of the total deposition at the Florida sites during our study period.

[54] Figure 12 (left) shows the monthly deposition averaged over 2006–2008 for the model at two locations covering the measurement sites in Florida detailed by *Prospero et al.* [2010]. The seasonality of deposition compares well with observations from these sites shown in Figure 3 of *Huneeus et al.* [2011]. While the majority of AEROCOM models in the *Huneeus et al.* [2011] comparison underestimate the magnitude of the deposition during summer considerably, we find that GEOS-Chem deposition totals are comparable to the observations. However, we do note that the deposition is considerably lower at the most northern site in Florida. Assuming that the 1994–1996 observations are representative of most years this indicates that, although the seasonality of dust deposited in Florida is well represented by the model, wet removal of dust may be too intense as it is transported northward.

[55] Comparison between model and MODIS transects in Figure 8 indicated that the model was removing too much aerosol across the Atlantic outflow region. Dry deposition may be contributing to this close to source but differences downwind can most likely be attributed to wet processes. The convective removal parameterization is dependent upon the rate constant for conversion of cloud condensate and the updraft velocity [*Jacob*, 2000]. In the GEOS-Chem model the conversion rate, k, is fixed at 5.0×10^{-3} s^{-1}, and *Liu et al.* [2001] have shown that the removal fraction is relatively insensitive to changes in updraft velocity (fixed at 5 ms^{-1} over ocean and 10 ms^{-1} over land). The model convective removal parameterization is very efficient at scavenging aerosol, with 40% and 63% of aerosol removed during 1 km of vertical transport over land and ocean, respectively. We also find that the simulated AOD is relatively insensitive to the fraction of aerosol removed each time step. Reducing the scavenging efficiency by 50% has almost no impact upon the daily AOD. This is likely to be a result of convective removal occurring over several model time steps, therefore the removal process is often saturated, resulting in close to 100% of the aerosol being scavenged during the convection event.

[56] Figure 13 compares the GEOS-5 model rainfall with observations made by the TRMM Microwave Imager (TMI). TMI products include precipitation rate and precipitation frequency on a 5° by 5° grid between 30°N and 30°S. The precipitation frequency is calculated by using a lognormal fit and delta function (to account for retrievals free of

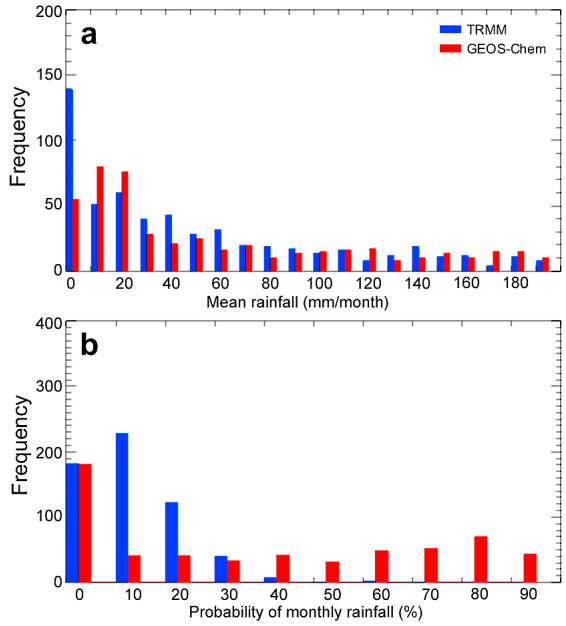

Figure 13. (top) The frequency of different intensity rainfall events averaged over the year for 5° × 5° regions across the dust outflow region is shown for TMI observations (blue lines) and the model (red lines). (bottom) The percentage of days with rainfall for each grid box in the outflow region is shown.

precipitation) to each 5° by 5° region. These are a composite of 69 × 43 km resolution observations made during morning and afternoon overpasses [*Wilheit et al.*, 1991]. Figure 13 shows the annual precipitation rate and precipitation probability for both the model and the observations averaged over 5° by 5° regions between 50°W–0°E and 5°S–20°N for 2006. We have used a threshold of 1 mm d^{-1} and consider all cases in the model below that as nonprecipitating to account for the sensitivity of the observations. We find that the total precipitation compares reasonably well for precipitation rates of over 40 mm $month^{-1}$ (Figure 13a). However, the model consistently underestimates the occurrence of near-zero rain rates and overestimates the occurrence of rates between 10 and 30 mm $month^{-1}$. This is further reinforced by the rain frequency data (Figure 13b) that show considerable differences in the probability distribution of rain between the model and the TMI observations. The observations indicate that the probability of it raining is less than 20% for the majority of the outflow region. In contrast, the model shows a relatively even distribution of rain probabilities with almost half of locations having rain on a daily basis. Although there is considerable uncertainty in the rainfall probability retrievals this may indicate that while the total rainfall in the model is reasonable, light rain occurs more frequently in the model than TMI observations suggest. In the model convective removal is independent of the rain rate, hence the frequency of rain is more important than the intensity of the rain for this process. For large-scale rain events both the frequency and the rate of precipitation is important. However, we find that even during the lightest rain events approximately 10%–40% of aerosol is removed per 15 min time step. Diagnosing these light rain events correctly poses a problem to global models and is a key uncertainty when modeling the long-range transport of aerosol.

5. Dust Transport: Deposition to the Atlantic, Amazon, and Caribbean

[57] To characterize the impact of dust upon the oceans and biosphere as a nutrient source and also understand potential air quality impacts it is useful to determine the deposition. The 3 year mean dust deposition totals for the model are 1377 ± 144 Tg yr^{-1} globally and 749 ± 114 Tg yr^{-1} for African dust (Table 3). These totals are both similar to the medians from the 14 AEROCOM models which show a wide range of deposition totals for the year 2000 [*Huneeus et al.*, 2011]. Globally, wet deposition accounts for 53% of all dust deposition, which is within the range of the AEROCOM models (16%–55%) used by *Prospero et al.* [2010].

[58] African dust concentrations have been sampled at Barbados (13°N, 59°W) since the 1960s [*Prospero and Nees*, 1986] now using a standard Atmosphere/Ocean Chemistry Experiment (AEROCE) 20 m tower. These invaluable daily dust measurements have been used to produce monthly mean dust concentrations to compare with the model over the 2006–2008 period. Figure 14 shows the time series for both model and in situ measurements. The summertime peak is captured in the model, especially in 2007 and 2008, but the model does somewhat underestimate the dust concentration during the fall season (but differences are within the observed standard deviations) and also in summer during 2006. However, the overall record at Barbados is well reproduced by the model, with a correlation of 0.74 for the entire period. The observed standard deviations are large for many of the months owing to the sporadic nature of the dust arrival from across the Atlantic. However, the model captures this variability well with monthly standard deviations in dust concentration comparable to those observed. Although this is only one site it indicates the model is able to represent the seasonality of dust transport to the Caribbean.

[59] Several studies have shown that a significant amount of African dust is transported to the Amazon, primarily

Table 3. Seasonal Dust Deposition Totals Calculated From GEOS-Chem Shown for the Amazon, Caribbean, and Atlantic Regions[a]

2006–2008	Amazon	Caribbean	Atlantic	African	Global
DJF	3.7 ± 2.6	0.4 ± 0.1	67.2 ± 29.1	202.9 ± 54.9	284.9 ± 54.8
MAM	7.9 ± 1.5	3.4 ± 1.4	54.6 ± 9.5	248.8 ± 38.2	453.2 ± 52.8
JJA	5.2 ± 1.0	21.0 ± 2.7	62.4 ± 13.1	171.3 ± 13.9	419.4 ± 30.3
SON	0.5 ± 0.5	1.4 ± 1.0	33.9 ± 1.0	126.4 ± 9.3	219.6 ± 14.9
Total	17.3 ± 5.0	26.3 ± 4.7	218.4 ± 47.6	749.4 ± 113.5	1377.1 ± 143.9

[a]Regions are as defined in Figure 15a. Totals are in Tg yr^{-1}. The deposition totals for all African dust and for all global dust are also shown. The results are 3 year averages (2006–2008) with the standard deviation between years.

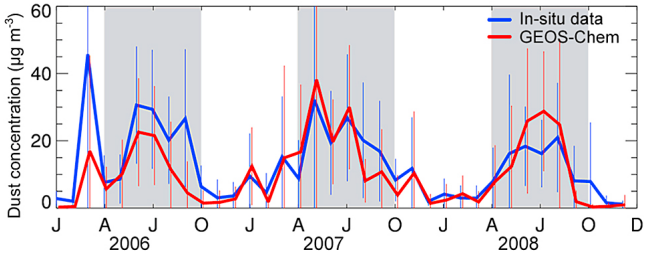

Figure 14. Time series of monthly dust concentration measurements at the surface site in Barbados (13°N, 60°W) for both GEOS-Chem (red line) and in situ measurements (blue line). Error bars indicate standard deviation of daily dust concentration used to create monthly average for both model and observations.

between March and May. It has been estimated that 50 Tg of mineral dust would be required, annually, to maintain the nutrient levels measured in the Amazon rain forests [*Swap et al.*, 1992]. Figure 15 shows the annual deposition of dust to the Americas. To estimate the nutrients deposited we assume there to be 700 μg of phosphorus per gram of dust in accordance with *Mahowald et al.* [2005a] and *Chadwick et al.* [1999], and similar to the 780 μg of phosphorus per gram of dust measured by *Bristow et al.* [2010] for dust from the Bodélé region. We find very similar results for the phosphorus deposited to the northernmost parts of the Amazon as *Mahowald et al.* [2005a] with their MATCH model, although we see a sharper latitudinal gradient as the amount of phosphorus decreases to near zero below 10°S. The sharp latitudinal gradient impacts the total amount of dust deposited to the Amazon considerably. This may

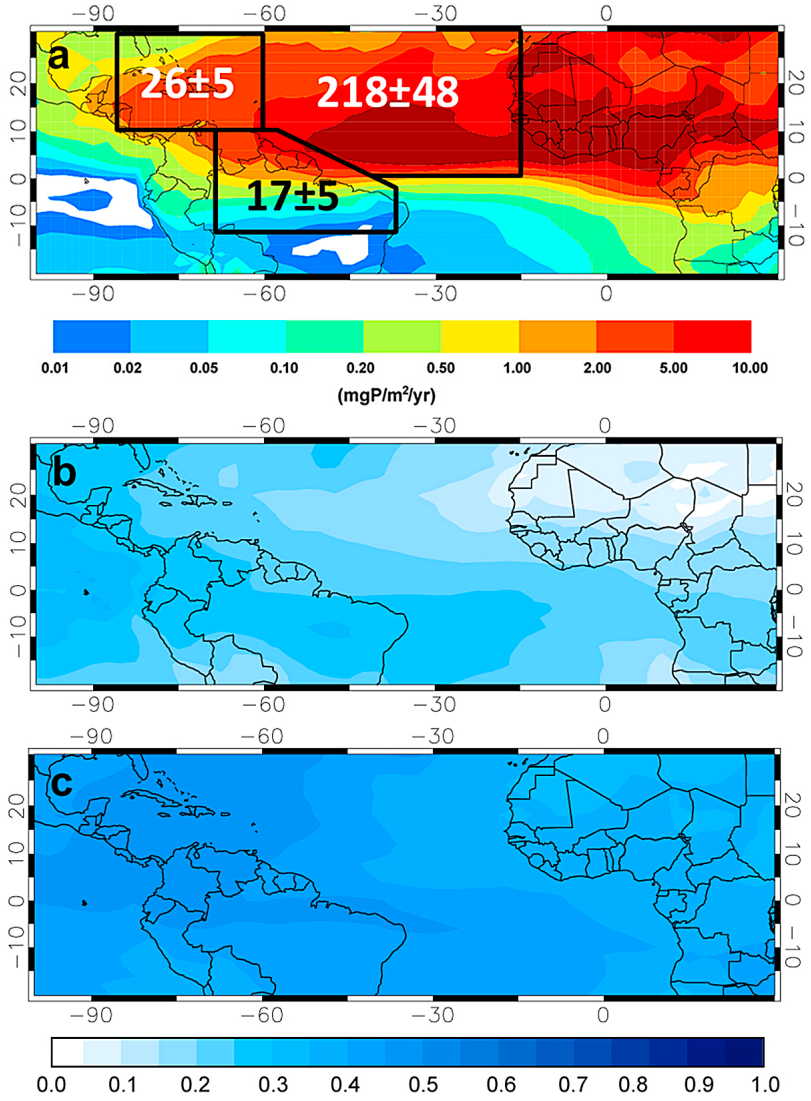

Figure 15. (a) The average annual amount of phosphorus (P) deposited is shown, based on the GEOS-Chem simulation from 2006 to 2008. The boxes show the regions considered when calculating the deposition to the Caribbean and Amazon. Totals inside the boxes are Tg of dust deposited over the year (proportional to the P deposited), with the error representing the interannual variability. (b) The fraction of the mass deposited in the submicron size range is shown, and (c) the fraction of the AOD from submicron dust is also shown. Note that the lower two plots share the same color bar.

indicate difficulty in transporting dust southward during the winter and spring, a common feature in the majority of the AEROCOM models [*Huneeus et al.*, 2011]. The submicron proportion of the dust mass deposited and the dust AOD are also shown (Figures 15b and 15c, respectively). Close to source the submicron dust contributes little to the total dust mass (<20%) while it still contributes at least half of the AOD from dust. Further downwind we see that 70%–80% of dust arriving in the Americas still comprises of dust greater than 2 μm in diameter, and up to 5% of the mass is from dust greater than 6 μm. Dust between 2 μm and 10 μm in diameter has been observed in the Amazon [*Formenti et al.*, 2001; *Martin et al.*, 2010], confirming this long-range transport of supermicron dust aerosol. *Cakmur et al.* [2006] show that clay makes up approximately 14% of the total dust by objective analysis which is similar to our results. However, they indicate that the ratio of submicron dust (clay) to supermicron dust (silt) stays relatively constant away from source suggesting that more silt maybe transported far from source than in our model.

[60] In Figure 15 the annual dust deposition is shown for three regions, averaged over the 3 years of the simulation. The total westward export is approximately 260 ± 55 Tg yr^{-1} based on 2006–2008 emissions. This represents 35% of the total African dust deposition, agreeing well with previous simulations [*Laurent et al.*, 2010]. The deposition total is slightly higher than estimates based on MODIS from 2001 (240 ± 80 Tg yr^{-1} from *Kaufman et al.* [2005]) but is still well within the uncertainty limits. The amount of dust deposited to the oceans in GEOS-Chem is 218 ± 48 Tg yr^{-1}, higher than the range 140–205 Tg yr^{-1} from previous studies [*Fan et al.*, 2004; *Ginoux et al.*, 2004; *Prospero et al.*, 1996] although the actual total is still quite uncertain. We estimate that 17 Tg $\pm$ 5 Tg of dust is annually deposited to the Amazon, considerably less than the satellite-based estimate of 50 Tg yr^{-1}. Evidence from comparison with TRMM, MODIS and CALIOP suggest that wet removal in the model is too strong, especially in the spring, therefore the modeled deposition to the Amazon can be considered a lower limit. However, switching off convective removal entirely for 2006 only increases the deposition to the Amazon by 54% (for 2006). *Koren et al.* [2006] estimate that 50% of the dust arriving in the Amazon is from the Bodélé region. We find that the Bodélé region contributes about 10% based on our model and this is relatively insensitive to doubling the emissions from the Bodélé depression. Thus, while our estimate of deposition to the Amazon remains a lower limit, the total is not likely to exceed our estimate by more than 50%.

6. Conclusions

[61] In this paper we have used satellite and ground-based observations to illustrate the characteristics of African dust export on daily to multiannual time scales. This has been used to investigate how the GEOS-Chem global model captures the processes required to simulate long-range transport of dust.

[62] Introducing a realistic submicron dust aerosol size distribution reduces the AOD due to dust aerosol by up to 25% (while conserving total mass) decreasing the RMS error between model and observations at all AERONET sites. We have shown that GEOS-Chem captures the seasonality of African dust emission but appears to overestimate the AOD during summer near the West African coast and underestimate the emissions from the Bodélé Depression. Increasing the emissions in the Bodélé Depression by a factor of two significantly reduces the RMS error with MODIS and MISR AOD and increases the correlation, suggesting that source function or the model winds may not be strong enough in this important region.

[63] Comparisons with CALIOP observations indicate that the model is able to represent the seasonality of the aerosol vertical structure and also the descending of the summer dust plumes as they cross the Atlantic. However, differences are apparent over the surface of the ocean, where CALIOP observes high extinction that the model is not capturing.

[64] We calculate global and African dust deposition totals (Table 3) and find them in good agreement with the medians of the ensemble of AEROCOM models. The total amount of dust to be exported westward from Africa to be 260 ± 55 Tg yr^{-1} which is comparable to values derived from satellite data. However, the amount deposited into the Atlantic is 218 ± 48 Tg yr^{-1} is toward the high end of previous studies. We find that only 17 ± 5 Tg yr^{-1} reach the Amazon which is considerably less than the 50 Tg yr^{-1} estimated from MODIS. Dust concentrations reaching the Caribbean agree well with the limited observations and comparison with deposition measurements in Florida show good seasonality and reasonable deposition totals at the southernmost location. This suggests that the lack of dust deposition to the Amazon may be the result of a seasonal bias in the model or more intense removal during the southward export pathway in spring – this discrepancy was highlighted for AEROCOM models also [*Huneeus et al.*, 2011]. Switching off convective removal entirely in the model still results in less than half the MODIS-derived dust reaching the Amazon, indicating that the satellite estimate of 50 Tg yr^{-1} may be too high. Comparison with MODIS optical depth across the outflow region indicates that the model dust lifetime is 25%–50% less than observed as it is transported across the Atlantic, especially in the spring months when transport to the Amazon occurs. Wet removal via nucleation scavenging and convective updraft scavenging is the likely cause of the excess removal. However, reducing the scavenging efficiency has little impact on the removal unless reduced unrealistically by more than 50%. Comparison of rainfall in the model with observations from the TRMM satellite indicate that although the total precipitation and strong rain events are well represented, light rain occurs more frequently in the model than the observations suggest. This may explain the model removing more aerosol than expected and demonstrates the challenges of developing realistic removal mechanisms in global models. Progress has been made in representing the dust emissions correctly and also highlighting issues that affect long-range transport of dust in global models. Further work is required to better understand the impact of excessive removal on dust radiative effects in clean remote regions, and also the impact of future changes in dust loading on ecosystems and air quality downwind.

[65] **Acknowledgments.** This work was partially supported by Colorado State University and by NASA grant NNX08AN75G. We thank the PIs D. Tanré, R. Ramos, E. Cuevas-Agullo, A. Diall, B. Chatenet, and J. L. Rajot for their effort in establishing and maintaining the AERONET

sites used in this study. We would also like to thank J. Huang for his help and thoughts relating to the MODIS Terra Deep Blue data, R. Kahn for his input on the MISR and MODIS data, and C. Kummerow and T. Wilheit for their input with the TMI data. The MODIS data were obtained from NASA Goddard Data Center, and MISR and CALIPSO data were obtained from the NASA Langley Research Centre Atmospheric Sciences Data Center.

References

Alexander, B., R. J. Park, D. J. Jacob, Q. B. Li, R. M. Yantosca, J. Savarino, C. C. W. Lee, and M. H. Thiemens (2005), Sulfate formation in sea-salt aerosols: Constraints from oxygen isotopes, *J. Geophys. Res.*, *110*, D10307, doi:10.1029/2004JD005659.

Alheit, R. R., et al. (1990), A theoretical-study of the wet removal of atmospheric pollutants. 4. The uptake and redistribution of aerosol-particles through nucleation and impaction scavenging by growing cloud drops and ice particles, *J. Atmos. Sci.*, *47*, 870–887, doi:10.1175/1520-0469(1990)047<0870:ATSOTW>2.0.CO;2.

Ben-Ami, Y., et al. (2010), Transport of North African dust from the Bodélé depression to the Amazon Basin: A case study, *Atmos. Chem. Phys.*, *10*, 7533–7544, doi:10.5194/acp-10-7533-2010.

Bonan, G. B. (1996), Sensitivity of a GCM simulation to subgrid infiltration and surface runoff, *Clim. Dyn.*, *12*, 279–285, doi:10.1007/BF00219501.

Bristow, C. S., K. A. Hudson-Edwards, and A. Chappell (2010), Fertilizing the Amazon and equatorial Atlantic with West African dust, *Geophys. Res. Lett.*, *37*, L14807, doi:10.1029/2010GL043486.

Cakmur, R. V., R. L. Miller, J. Perlwitz, I. V. Geogdzhayev, P. Ginoux, D. Koch, K. E. Kohfeld, I. Tegen, and C. S. Zender (2006), Constraining the magnitude of the global dust cycle by minimizing the difference between a model and observations, *J. Geophys. Res.*, *111*, D06207, doi:10.1029/2005JD005791.

Chadwick, O. A., et al. (1999), Changing sources of nutrients during four million years of ecosystem development, *Nature*, *397*, 491–497, doi:10.1038/17276.

Christopher, S. A., et al. (2011), Multi-sensor satellite remote sensing of dust aerosols over North Africa during GERBILS, *Q. J. R. Meteorol. Soc.*, *137*, 1168–1178, doi:10.1002/qj.863.

Chu, D. A., Y. J. Kaufman, C. Ichoku, L. A. Remer, D. Tanré, and B. N. Holben (2002), Validation of MODIS aerosol optical depth retrieval over land, *Geophys. Res. Lett.*, *29*(12), 8007, doi:10.1029/2001GL013205.

Croft, B., et al. (2010), Influences of in-cloud aerosol scavenging parameterizations on aerosol concentrations and wet deposition in ECHAM5-HAM, *Atmos. Chem. Phys.*, *10*, 1511–1543, doi:10.5194/acp-10-1511-2010.

d'Almeida, G. A. (1986), A model for Saharan dust transport, *J. Clim. Appl. Meteorol.*, *25*, 903–916, doi:10.1175/1520-0450(1986)025<0903:AMFSDT>2.0.CO;2.

Di Girolamo, L., T. C. Bond, D. Bramer, D. J. Diner, F. Fettinger, R. A. Kahn, J. V. Martonchik, M. V. Ramana, V. Ramanathan, and P. J. Rasch (2004), Analysis of Multi-angle Imaging SpectroRadiometer (MISR) aerosol optical depths over greater India during winter 2001–2004, *Geophys. Res. Lett.*, *31*, L23115, doi:10.1029/2004GL021273.

Di Pierro, M. D. P. M., et al. (2011), Satellite observations of aerosol transport from East Asia to the Arctic: Three case studies, *Atmos. Chem. Phys.*, *11*, 2225–2243, doi:10.5194/acp-11-2225-2011.

Drury, E., et al. (2010), Synthesis of satellite (MODIS), aircraft (ICARTT), and surface (IMPROVE, EPA-AQS, AERONET) aerosol observations over eastern North America to improve MODIS aerosol retrievals and constrain surface aerosol concentrations and sources, *J. Geophys. Res.*, *115*, D14204, doi:10.1029/2009JD012629.

Eck, T. F., et al. (2003), Variability of biomass burning aerosol optical characteristics in southern Africa during the SAFARI 2000 dry season campaign and a comparison of single scattering albedo estimates from radiometric measurements, *J. Geophys. Res.*, *108*(D13), 8477, doi:10.1029/2002JD002321.

Eguchi, K., et al. (2009), Trans-Pacific dust transport: Integrated analysis of NASA/CALIPSO and a global aerosol transport model, *Atmos. Chem. Phys.*, *9*, 3137–3145, doi:10.5194/acp-9-3137-2009.

Fairlie, T. D., et al. (2007), The impact of transpacific transport of mineral dust in the United States, *Atmos. Environ.*, *41*, 1251–1266, doi:10.1016/j.atmosenv.2006.09.048.

Fan, S. M., L. W. Horowitz, H. Levy II, and W. J. Moxim (2004), Impact of air pollution on wet deposition of mineral dust aerosols, *Geophys. Res. Lett.*, *31*, L02104, doi:10.1029/2003GL018501.

Fisher, J. A., et al. (2011), Sources, distribution, and acidity of sulfate-ammonium aerosol in the Arctic in winter-spring, *Atmos. Environ.*, *45*, 7301–7318, doi:10.1016/j.atmosenv.2011.08.030.

Flossmann, A. I., and H. R. Pruppacher (1989), A theoretical-study of the wet removal of atmospheric pollutants. 1. The redistribution of aerosol-particles captured through nucleation and impaction scavenging by growing cloud drops, and. 2. The uptake and redistribution of $(NH_4)^2SO_4$ particles and SO_2 gas simultaneously scavenged by growing cloud drops—Reply, *J. Atmos. Sci.*, *46*, 1870–1871, doi:10.1175/1520-0469(1989)046<1870:R>2.0.CO;2.

Formenti, P., M. O. Andreae, L. Lange, G. Roberts, J. Cafmeyer, I. Rajta, W. Maenhaut, B. N. Holben, P. Artaxo, and J. Lelievel (2001), Saharan dust in Brazil and Suriname during the Large-Scale Biosphere-Atmosphere Experiment in Amazonia (LBA)–Cooperative LBA Regional Experiment (CLAIRE) in March 1998, *J. Geophys. Res.*, *106*, 14,919–14,934, doi:10.1029/2000JD900827.

Generoso, S., I. Bey, M. Labonne, and F.-M. Bréon (2008), Aerosol vertical distribution in dust outflow over the Atlantic: Comparisons between GEOS-Chem and Cloud-Aerosol Lidar and Infrared Pathfinder Satellite Observation (CALIPSO), *J. Geophys. Res.*, *113*, D24209, doi:10.1029/2008JD010154.

Giglio, L., et al. (2003), An enhanced contextual fire detection algorithm for MODIS, *Remote Sens. Environ.*, *87*, 273–282, doi:10.1016/S0034-4257(03)00184-6.

Gillette, D. A., and R. Passi (1988), Modeling dust emission caused by wind erosion, *J. Geophys. Res.*, *93*, 14,233–14,242, doi:10.1029/JD093iD11p14233.

Ginoux, P., M. Chin, I. Tegen, J. M. Prospero, B. Holben, O. Dubovik, and S.-J. Lin (2001), Sources and distributions of dust aerosols simulated with the GOCART model, *J. Geophys. Res.*, *106*, 20,255–20,273, doi:10.1029/2000JD000053.

Ginoux, P., et al. (2004), Long-term simulation of global dust distribution with the GOCART model: Correlation with North Atlantic Oscillation, *Environ. Model. Softw.*, *19*, 113–128, doi:10.1016/S1364-8152(03)00114-2.

Gyan, K., et al. (2005), African dust clouds are associated with increased paediatric asthma accident and emergency admissions on the Caribbean island of Trinidad, *Int. J. Biometeorol.*, *49*, 371–376, doi:10.1007/s00484-005-0257-3.

Haywood, J., et al. (2003a), Radiative properties and direct radiative effect of Saharan dust measured by the C-130 aircraft during SHADE: 1. Solar spectrum, *J. Geophys. Res.*, *108*(D18), 8577, doi:10.1029/2002JD002687.

Haywood, J. M., S. R. Osborne, P. N. Francis, A. Keil, P. Formenti, M. O. Andreae, and P. H. Kaye (2003b), The mean physical and optical properties of regional haze dominated by biomass burning aerosol measured from the C-130 aircraft during SAFARI 2000, *J. Geophys. Res.*, *108*(D13), 8473, doi:10.1029/2002JD002226.

Haywood, J. M., et al. (2008), Overview of the Dust and Biomass-burning Experiment and African Monsoon Multidisciplinary Analysis Special Observing Period-0, *J. Geophys. Res.*, *113*, D00C17, doi:10.1029/2008JD010077.

Henze, D. K., et al. (2008), Global modeling of secondary organic aerosol formation from aromatic hydrocarbons: High- vs. low-yield pathways, *Atmos. Chem. Phys.*, *8*, 2405–2420, doi:10.5194/acp-8-2405-2008.

Highwood, E. J., J. M. Haywood, M. D. Silverstone, S. M. Newman, and J. P. Taylor (2003), Radiative properties and direct effect of Saharan dust measured by the C-130 aircraft during Saharan Dust Experiment (SHADE): 2. Terrestrial spectrum, *J. Geophys. Res.*, *108*(D18), 8578, doi:10.1029/2002JD002552.

Holben, B., et al. (1998), AERONET—A federated instrument network and data archive for aerosol characterization, *Remote Sens. Environ.*, *66*, 1–16, doi:10.1016/S0034-4257(98)00031-5.

Hsu, N. C., et al. (2006), Deep blue retrievals of Asian aerosol properties during ACE-Asia, *IEEE Trans. Geosci. Remote Sens.*, *44*, 3180–3195, doi:10.1109/TGRS.2006.879540.

Huang, J. F., C. Zhang, and J. M. Prospero (2010), African dust outbreaks: A satellite perspective of temporal and spatial variability over the tropical Atlantic Ocean, *J. Geophys. Res.*, *115*, D05202, doi:10.1029/2009JD012516.

Huneeus, N., et al. (2011), Global dust model intercomparison in AeroCom phase I, *Atmos. Chem. Phys.*, *11*, 7781–7816, doi:10.5194/acp-11-7781-2011.

Jacob, D. J. (2000), Heterogeneous chemistry and tropospheric ozone, *Atmos. Environ.*, *34*, 2131–2159, doi:10.1016/S1352-2310(99)00462-8.

Jaeglé, L., et al. (2010), Global distribution of sea salt aerosols: New constraints from in situ and remote sensing observations, *Atmos. Chem. Phys. Discuss.*, *10*, 25,687–25,742, doi:10.5194/acpd-10-25687-2010.

Jickells, T. D., et al. (2005), Global iron connections between desert dust, ocean biogeochemistry, and climate, *Science*, *308*, 67–71, doi:10.1126/science.1105959.

Kahn, R. A., B. J. Gaitley, J. V. Martonchik, D. J. Diner, K. A. Crean, and B. Holben (2005), Multiangle Imaging Spectroradiometer (MISR) global aerosol optical depth validation based on 2 years of coincident Aerosol Robotic Network (AERONET) observations, *J. Geophys. Res.*, *110*, D10S04, doi:10.1029/2004JD004706.

Kahn, R. A., M. J. Garay, D. L. Nelson, K. K. Yau, M. A. Bull, B. J. Gaitley, J. V. Martonchik, and R. C. Levy (2007), Satellite-derived aerosol optical depth over dark water from MISR and MODIS: Comparisons with AERONET and implications for climatological studies, *J. Geophys. Res.*, *112*, D18205, doi:10.1029/2006JD008175.

Kahn, R. A., et al. (2009), MISR aerosol product attributes and statistical comparisons with MODIS, *IEEE Trans. Geosci. Remote Sens.*, *47*, 4095–4114, doi:10.1109/TGRS.2009.2023115.

Kahn, R. A., B. J. Gaitley, M. J. Garay, D. J. Diner, T. F. Eck, A. Smirnov, and B. N. Holben (2010), Multiangle Imaging SpectroRadiometer global aerosol product assessment by comparison with the Aerosol Robotic Network, *J. Geophys. Res.*, *115*, D23209, doi:10.1029/2010JD014601.

Kahn, R. A., et al. (2011), Response to "Toward unified satellite climatology of aerosol properties. 3. MODIS versus MISR versus AERONET," *J. Quant. Spectrosc. Radiat. Transf.*, *112*, 901–909, doi:10.1016/j.jqsrt.2010.11.001.

Kalashnikova, O. V., and R. A. Kahn (2008), Mineral dust plume evolution over the Atlantic from MISR and MODIS aerosol retrievals, *J. Geophys. Res.*, *113*, D24204, doi:10.1029/2008JD010083.

Kalashnikova, O. V., et al. (2011), Climatological analysis of MISR, MODIS and OMI aerosol products in East Asian dust source regions, paper M240A presented at the World Climate Research Programme Conference, World Meteorol. Soc, Dener, Colo.

Kaufman, Y. J., I. Koren, L. A. Remer, D. Tanré, P. Ginoux, and S. Fan (2005), Dust transport and deposition observed from the Terra-Moderate Resolution Imaging Spectroradiometer (MODIS) spacecraft over the Atlantic Ocean, *J. Geophys. Res.*, *110*, D10S12, doi:10.1029/2003JD004436.

Kinne, S., et al. (2003), Monthly averages of aerosol properties: A global comparison among models, satellite data, and AERONET ground data, *J. Geophys. Res.*, *108*(D20), 4634, doi:10.1029/2001JD001253.

Knippertz, P. (2008), Dust emissions in the West African heat trough—The role of the diurnal cycle and of extratropical disturbances, *Meteorol. Z.*, *17*, 553–563, doi:10.1127/0941-2948/2008/0315.

Kopke, P., et al. (1997), *Global Aerosol Data Set*, Max Planck Inst. for Meteorol., Hamburg, Germany.

Koren, I., et al. (2006), The Bodele depression: A single spot in the Sahara that provides most of the mineral dust to the Amazon forest, *Environ. Res. Lett.*, *1*(1), 014005, doi:10.1088/1748-9326/1/1/014005.

Lapina, K., et al. (2011), Investigating organic aerosol loading in the remote marine environment, *Atmos. Chem. Phys.*, *11*, 8847–8860, doi:10.5194/acp-11-8847-2011.

Laurent, B., I. Tegen, B. Heinold, K. Schepanski, B. Weinzierl, and M. Esselborn (2010), A model study of Saharan dust emissions and distributions during the SAMUM-1 campaign, *J. Geophys. Res.*, *115*, D21210, doi:10.1029/2009JD012995.

Levy, R. C., et al. (2005), Evaluation of the MODIS aerosol retrievals over ocean and land during CLAMS, *J. Atmos. Sci.*, *62*, 974–992, doi:10.1175/JAS3391.1.

Levy, R. C., et al. (2010), Global evaluation of the Collection 5 MODIS dark-target aerosol products over land, *Atmos. Chem. Phys.*, *10*, 10,399–10,420, doi:10.5194/acp-10-10399-2010.

Li, F., et al. (2004), Saharan dust aerosol radiative forcing measured from space, *J. Clim.*, *17*, 2558–2571, doi:10.1175/1520-0442(2004)017<2558:SDARFM>2.0.CO;2.

Liao, H., D. K. Henze, J. H. Seinfeld, S. Wu, and L. J. Mickley (2007), Biogenic secondary organic aerosol over the United States: Comparison of climatological simulations with observations, *J. Geophys. Res.*, *112*, D06201, doi:10.1029/2006JD007813.

Liu, H. Y., D. J. Jacob, I. Bey, and R. M. Yantosca (2001), Constraints from Pb-210 and Be-7 on wet deposition and transport in a global three-dimensional chemical tracer model driven by assimilated meteorological fields, *J. Geophys. Res.*, *106*, 12,109–12,128, doi:10.1029/2000JD900839.

Mahowald, N. M., P. Artaxo, A. R. Baker, T. D. Jickells, G. S. Okin, J. T. Randerson, and A. R. Townsend (2005a), Impacts of biomass burning emissions and land use change on Amazonian atmospheric phosphorus cycling and deposition, *Global Biogeochem. Cycles*, *19*, GB4030, doi:10.1029/2005GB002541.

Mahowald, N. M., A. R. Baker, G. Bergametti, N. Brooks, R. A. Duce, T. D. Jickells, N. Kubilay, J. M. Prospero, and I. Tegen (2005b), Atmospheric global dust cycle and iron inputs to the ocean, *Global Biogeochem. Cycles*, *19*, GB4025, doi:10.1029/2004GB002402.

Marsham, J. H., D. J. Parker, C. M. Grams, C. M. Taylor, and J. M. Haywood (2008), Uplift of Saharan dust south of the intertropical discontinuity, *J. Geophys. Res.*, *113*, D21102, doi:10.1029/2008JD009844.

Marsham, J. H., P. Knippertz, N. S. Dixon, D. J. Parker, and G. M. S. Lister (2011), The importance of the representation of deep convection for modeled dust-generated winds over West Africa during summer, *Geophys. Res. Lett.*, *38*, L16803, doi:10.1029/2011GL048368.

Martet, M., et al. (2009), Evaluation of long-range transport and deposition of desert dust with the CTM MOCAGE, *Tellus, Ser. B*, *61*, 449–463, doi:10.1111/j.1600-0889.2008.00413.x.

Marticorena, B., G. Bergametti, B. Aumont, Y. Callot, C. N'Doumé, and M. Legrand (1997), Modeling the atmospheric dust cycle. 2. Simulation of Saharan dust sources, *J. Geophys. Res.*, *102*, 4387–4404, doi:10.1029/96JD02964.

Martin, R. V., D. J. Jacob, R. M. Yantosca, M. Chin, and P. Ginoux (2003), Global and regional decreases in tropospheric oxidants from photochemical effects of aerosols, *J. Geophys. Res.*, *108*(D3), 4097, doi:10.1029/2002JD002622.

Martin, S. T., et al. (2010), Sources and properties of Amazonian aerosol particles, *Rev. Geophys.*, *48*, RG2002, doi:10.1029/2008RG000280.

Martonchik, J. V., et al. (1998), Techniques for the retrieval of aerosol properties over land and ocean using multiangle imaging, *IEEE Trans. Geosci. Remote Sens.*, *36*, 1212–1227, doi:10.1109/36.701027.

Martonchik, J. V., et al. (2002), Regional aerosol retrieval results from MISR, *IEEE Trans. Geosci. Remote Sens.*, *40*, 1520–1531, doi:10.1109/TGRS.2002.801142.

Martonchik, J. V., D. J. Diner, R. Kahn, B. Gaitley, and B. N. Holben (2004), Comparison of MISR and AERONET aerosol optical depths over desert sites, *Geophys. Res. Lett.*, *31*, L16102, doi:10.1029/2004GL019807.

Mbourou, G. N., et al. (1997), The diurnal and seasonal cycles of windborne dust over Africa north of the equator, *J. Appl. Meteorol.*, *36*, 868–882, doi:10.1175/1520-0450(1997)036<0868:TDASCO>2.0.CO;2.

Nickovic, S., et al. (2000), Simulation and measurements of dust deposition in Macedonia, in *Nucleation and Atmospheric Aerosols 2000*, edited by B. N. Hale and M. Kulmala, pp. 530–533, Am. Inst. Phys., Melville, N. Y.

Osborne, S. R., B. T. Johnson, J. M. Haywood, A. J. Baran, M. A. J. Harrison, and C. L. McConnell (2008), Physical and optical properties of mineral dust aerosol during the Dust and Biomass-burning Experiment, *J. Geophys. Res.*, *113*, D00C03, doi:10.1029/2007JD009551.

Park, R. J., D. J. Jacob, M. Chin, and R. V. Martin (2003), Sources of carbonaceous aerosols over the United States and implications for natural visibility, *J. Geophys. Res.*, *108*(D12), 4355, doi:10.1029/2002JD003190.

Park, R. J., D. J. Jacob, B. D. Field, R. M. Yantosca, and M. Chin (2004), Natural and transboundary pollution influences on sulfate-nitrate-ammonium aerosols in the United States: Implications for policy, *J. Geophys. Res.*, *109*, D15204, doi:10.1029/2003JD004473.

Prospero, J. M. (1999), Long-term measurements of the transport of African mineral dust to the southeastern United States: Implications for regional air quality, *J. Geophys. Res.*, *104*, 15,917–15,927, doi:10.1029/1999JD900072.

Prospero, J. M., and R. T. Nees (1986), Impact of the North African drought and El-Nino on mineral dust in the Barbados trade winds, *Nature*, *320*, 735–738, doi:10.1038/320735a0.

Prospero, J. M., et al. (1981), Atmospheric transport of soil dust from Africa to South-America, *Nature*, *289*, 570–572, doi:10.1038/289570a0.

Prospero, J. M., et al. (1996), Atmospheric deposition of nutrients to the North Atlantic Basin, *Biogeochemistry*, *35*, 27–73, doi:10.1007/BF02179824.

Prospero, J. M., et al. (2001), Al and Fe in PM 2.5 and PM 10 suspended particles in south-central Florida: The impact of the long range transport of African mineral dust, *Water Air Soil Pollut.*, *125*, 291–317, doi:10.1023/A:1005277214288.

Prospero, J. M., et al. (2005), Interhemispheric transport of viable fungi and bacteria from Africa to the Caribbean with soil dust, *Aerobiologia*, *21*, 1–19, doi:10.1007/s10453-004-5872-7.

Prospero, J. M., W. M. Landing, and M. Schulz (2010), African dust deposition to Florida: Temporal and spatial variability and comparisons to models, *J. Geophys. Res.*, *115*, D13304, doi:10.1029/2009JD012773.

Ravi, S., et al. (2011), Aeolian processes and the biosphere, *Rev. Geophys.*, *49*, RG3001, doi:10.1029/2010RG000328.

Reid, J. S., et al. (2003), Analysis of measurements of Saharan dust by airborne and ground-based remote sensing methods during the Puerto Rico Dust Experiment (PRIDE), *J. Geophys. Res.*, *108*(D19), 8586, doi:10.1029/2002JD002493.

Remer, L. A., et al. (2002), Validation of MODIS aerosol retrieval over ocean, *Geophys. Res. Lett.*, *29*(12), 8008, doi:10.1029/2001GL013204.

Remer, L. A., et al. (2005a), The MODIS aerosol algorithm, products and validation, *J. Atmos. Sci*, *62*, 947–973.

Remer, L. A., et al. (2005b), *Algorithm for Remote Sensing of Tropospheric Aerosol from MODIS: Collection 5*, 87 pp., NASA Goddard Space Flight Cent., Greenbelt, Md.

Schepanski, K., et al. (2009a), Saharan dust transport and deposition towards the tropical northern Atlantic, *Atmos. Chem. Phys.*, *9*, 1173–1189, doi:10.5194/acp-9-1173-2009.

Schepanski, K., I. Tegen, M. C. Todd, B. Heinold, G. Bönisch, B. Laurent, and A. Macke (2009b), Meteorological processes forcing Saharan dust emission inferred from MSG-SEVIRI observations of subdaily dust source activation and numerical models, *J. Geophys. Res.*, *114*, D10201, doi:10.1029/2008JD010325.

Schulz, M., Y. J. Balkanski, W. Guelle, and F. Dulac (1998), Role of aerosol size distribution and source location in a three-dimensional simulation of a Saharan dust episode tested against satellite-derived optical thickness, *J. Geophys. Res.*, *103*, 10,579–10,592, doi:10.1029/97JD02779.

Shao, Y., and M. Raupach (1993), Effect of saltation bombardment by wind, *J. Geophys. Res.*, *98*, 12,719–12,726.

Smirnov, A., B. N. Holben, T. F. Eck, I. Slutsker, B. Chatenet, and R. T. Pinker (2002), Diurnal variability of aerosol optical depth observed at AERONET (Aerosol Robotic Network) sites, *Geophys. Res. Lett.*, *29*(23), 2115, doi:10.1029/2002GL016305.

Sokolik, I. N., and O. B. Toon (1996), Direct radiative forcing by anthropogenic airborne mineral aerosols, *Nature*, *381*, 681–683, doi:10.1038/381681a0.

Swap, R., et al. (1992), Saharan dust in the Amazon Basin, *Tellus, Ser. B*, *44*, 133–149, doi:10.1034/j.1600-0889.1992.t01-1-00005.x.

Tanré, D., et al. (2003), Measurement and modeling of the Saharan dust radiative impact: Overview of the Saharan Dust Experiment (SHADE), *J. Geophys. Res.*, *108*(D18), 8574, doi:10.1029/2002JD003273.

Tegen, I., and A. A. Lacis (1996), Modeling of particle size distribution and its influence on the radiative properties of mineral dust aerosol, *J. Geophys. Res.*, *101*, 19,237–19,244, doi:10.1029/95JD03610.

Tegen, I., et al. (2006), Modelling soil dust aerosol in the Bodele depression during the BoDEx campaign, *Atmos. Chem. Phys.*, *6*, 4345–4359, doi:10.5194/acp-6-4345-2006.

Tempel, P., et al. (1996), IGBP-DIS data set for pedotransfer function development, working paper, Int. Soil Ref. and Inf. Cent., Wageningen, Netherlands.

van der Werf, G. R., et al. (2003), Carbon emissions from fires in tropical and subtropical ecosystems, *Global Change Biol.*, *9*, 547–562, doi:10.1046/j.1365-2486.2003.00604.x.

Vaughan, M. (2004), Algorithm for retrieving lidar ratios at 1064 nm from space-based lidar backscatter data, *Proc. SPIE Int. Soc. Opt. Eng.*, *5240*, 104–115, doi:10.1117/12.510770.

Washington, R., and M. C. Todd (2005), Atmospheric controls on mineral dust emission from the Bodele Depression, Chad: The role of the low level jet, *Geophys. Res. Lett.*, *32*, L17701, doi:10.1029/2005GL023597.

Wilheit, T. T., et al. (1991), Retrieval of monthly rainfall indexes from microwave radiometric measurements using probability-distribution functions, *J. Atmos. Oceanic Technol.*, *8*, 118–136, doi:10.1175/1520-0426(1991)008<0118:ROMRIF>2.0.CO;2.

Young, S. A., and M. A. Vaughan (2009), The retrieval of profiles of particulate extinction from Cloud-Aerosol Lidar Infrared Pathfinder Satellite Observations (CALIPSO) data: Algorithm description, *J. Atmos. Oceanic Technol.*, *26*, 1105–1119, doi:10.1175/2008JTECHA1221.1.

Yu, H. B., M. Chin, D. M. Winker, A. H. Omar, Z. Liu, C. Kittaka, and T. Diehl (2010), Global view of aerosol vertical distributions from CALIPSO lidar measurements and GOCART simulations: Regional and seasonal variations, *J. Geophys. Res.*, *115*, D00H30, doi:10.1029/2009JD013364.

Zender, C. S., H. Bian, and D. Newman (2003a), Mineral Dust Entrainment and Deposition (DEAD) model: Description and 1990s dust climatology, *J. Geophys. Res.*, *108*(D14), 4416, doi:10.1029/2002JD002775.

Zender, C. S., D. Newman, and O. Torres (2003b), Spatial heterogeneity in aeolian erodibility: Uniform, topographic, geomorphic, and hydrologic hypotheses, *J. Geophys. Res.*, *108*(D17), 4543, doi:10.1029/2002JD003039.

Zhao, H. B., and C. G. Zheng (2006), Stochastic algorithm and numerical simulation for drop scavenging of aerosols, *Appl. Math. Mech.*, *27*, 1321–1332, doi:10.1007/s10483-006-1004-z.

B. Ford, C. L. Heald, and D. A. Ridley, Department of Atmospheric Science, Colorado State University, Fort Collins, CO 80523, USA. (daridley@atmos.colostate.edu)